

University of Louisville

## ThinkIR: The University of Louisville's Institutional Repository

---

Electronic Theses and Dissertations

---

12-2021

### An investigation into energy-material properties interaction in additive manufacturing of Polymers.

Pu Han

*University of Louisville*

Follow this and additional works at: <https://ir.library.louisville.edu/etd>



Part of the [Manufacturing Commons](#), and the [Polymer and Organic Materials Commons](#)

---

#### Recommended Citation

Han, Pu, "An investigation into energy-material properties interaction in additive manufacturing of Polymers." (2021). *Electronic Theses and Dissertations*. Paper 3799.

<https://doi.org/10.18297/etd/3799>

This Doctoral Dissertation is brought to you for free and open access by ThinkIR: The University of Louisville's Institutional Repository. It has been accepted for inclusion in Electronic Theses and Dissertations by an authorized administrator of ThinkIR: The University of Louisville's Institutional Repository. This title appears here courtesy of the author, who has retained all other copyrights. For more information, please contact [thinkir@louisville.edu](mailto:thinkir@louisville.edu).

AN INVESTIGATION INTO ENERGY-MATERIAL PROPERTIES INTERACTION  
IN ADDITIVE MANUFACTURING OF POLYMERS

By

Pu Han

A Dissertation

Submitted to the Faculty of the  
J.B. Speed School of Engineering of the University of Louisville  
in Fulfillment of the Requirements  
for the Degree of

Doctor of Philosophy  
in Mechanical Engineering

Department of Mechanical Engineering  
University of Louisville  
Louisville, Kentucky, United States

December 2021

Copyright by Pu Han

All rights reserve



AN INVESTIGATION INTO ENERGY-MATERIAL PROPERTIES INTERACTION  
IN ADDITIVE MANUFACTURING OF POLYMERS

By  
Pu Han

A Dissertation Approved on

November 29, 2021

by the following Dissertation Committee

.....  
Dr. Keng Hsu  
Dissertation Chairman

.....  
Dr. Dan Popa  
Dissertation Member

.....  
Dr. Kunal Kate  
Dissertation Member

.....  
Dr. Bikram Bhatia  
Dissertation Member

## DEDICATION

This dissertation is dedicated to my parents

Mrs. Yu-Ling Han

and

Mr. Yu-Hua Han

for their endless love, sacrifice, and guidance throughout my life

## ACKNOWLEDGEMENTS

First and foremost, I am extremely grateful to my PhD supervisor, Dr. Keng Hsu, for his invaluable mentorship and friendship throughout this journey. I cherish his personality and his altitude on research and study. He is more than an advisor or a professor, but a role model that I wish I could become in the future. His in-depth view and patience motivated me throughout my journey as a PhD student.

I greatly acknowledge my PhD committee members, Prof. Dan Popa, Prof. Kunal Kate and Prof. Bikram Bhatia, for taking time out of their busy schedule and delivering valuable criticism for my research, especially in the proposal defense. I would like to thank Dan Popa for guidance during my work in EPSCOR. I would like to thank Dr. Peter Quesada and Dr. Kevin Murphy for their help during my transition to University of Louisville.

I would also like to appreciate Dr. Jacek Jasinski at the Conn Center for his help with SEM and other characterization instruments. I would like to extend my gratitude to the Mechanical department, professors and the staffs, Dr. Sundar Atre, Dr. Srinivasan Rasipuram, John Jones and Diane Jenne, Curt McKenna.

I take this opportunity to thank my lab mates and colleagues Dr. Alireza Tofangchi, Dr. Anagh Deshpande, Sihan Zhang, Julio Izquierdo, Zhennan Zhang, Zhong Yang, Dr. Paramjot Singh, Kavish Sundan, Dr. Shanshan Zhang, Saleh Khanjar, Huan Jiang, Saransh

Gupta, Saumya Gulati, Ruoshi Zhang, and Danming Wei for their help and support throughout my time at University of Louisville.

I would like to thank my parents, Yu-Hua Han and Yu-Ling Han for their love and support.

I would like to thank my elder cousins Guoxi Han, Dongfeng Luan for their encouragement. I would like to thank my friends Qian Wan and Sirong Lu for their supporting during this journey.



## ABSTRACT

### AN INVESTIGATION INTO ENERGY-MATERIAL PROPERTIES INTERACTION IN ADDITIVE MANUFACTURING OF POLYMERS

Pu Han

November 29, 2021

Additive manufacturing (AM), known as three-dimensional (3D) printing, is a fabrication process to build 3D objects layer by layer based on computer aided design (CAD) model or digital 3D model. Fused filament fabrication (FFF) has become a preferred method for additive manufacturing due to its cost-effectiveness and flexibility. However, the parts built using FFF process suffer from lower mechanical strength compared to that fabricated using traditional method and rough surface finish.

With this motivation, this dissertation aims to develop and implement a novel in-process laser assisted technique on FFF to heal the microstructure of FFF built objects by enhancing reptation and relaxation to improve mechanical strength and to heal the surface by increasing surface reflow. This technique utilizes laser energy to reduce with residual stress generated by the extrusion-based deposition process, and to heal interfaces between deposited tracks for improvement of interface adhesion, therefore increase mechanical strength. This dissertation demonstrates that the in-process laser assisted technique can fabricate nearly isotropic object with mechanical strength close to solid bulk material. It also demonstrates the capability of reducing the surface roughness significantly.

This dissertation investigates in two directions, the first direction is mechanical strength and mechanical behaviors. In-process pre-laser heating was used to enhancing mechanical strength at inter-layer interface (Z-direction), at the interface between adjacent tracks (Y-direction), and along the deposited track(X-direction). The second direction is surface finish of the side surface. In order to quantify the interaction of laser energy on material structure, laser output power, laser melting pool temperature, mechanical strength were measured. SEM were used to characterize the fracture surface to determine the effect of laser on interface healing.

## TABLE OF CONTENTS

CHAPTER 1.....	1
INTRODUCTION .....	1
ChHAPTER 2.....	4
AN APPROACH TO IMPROVE INTERFACE HEALING IN FFF-3D PRINTED ULTEM 1010 USING LASER PRE-DEPOSITION HEATING.....	4
2.1 INTRODUCTION .....	4
2.2 METHODOLOGY .....	4
2.2.1 SAMPLE PREPARATION .....	4
2.2.2 LOCALIZED LASER PRE-HEATING APPARATUS.....	7
2.2.3 MECHANICAL TESTING-TENSILE STRENGTH.....	8
2.3 RESULTS AND DISCUSSION .....	9
2.4 CONCLUSIONS.....	15
CHAPTER 3.....	16
EFFECT OF IN-PROCESS LASER INTERFACE HEATING ON STRENGTH ISOTROPY OF EXTRUSION-BASED ADDITIVELY MANUFACTURED PEEK ....	16
3.1 INTRODUCTION .....	16
3.2 METHODOLOGY .....	18
3.2.1 LOCALIZED LASER PRE-HEATING APPARATUS.....	18

3.2.2 SAMPLE PREPARATION .....	19
3.2.3 MECHANICAL TESTING-TENSILE STRENGTH .....	22
3.3 RESULTS AND DISCUSSION .....	22
3.4 CONCLUSIONS.....	27
CHAPTER 4.....	28
RELAXATION OF RESIDUAL STRESS IN FUSED FILAMENT FABRICATION	
PART WITH IN-PROCESS LASER HEATING.....	
4.1 INTRODUCTION .....	28
4.2 MATERIALS AND METHODS.....	31
4.2.1 LASER PRE-HEATING APPARATUS .....	31
4.2.2 SAMPLE PREPARATION .....	33
4.2.3 MECHANICAL TEST .....	35
4.2.4 TEMPERATURE PROFILE .....	35
4.3 RESULTS AND DISCUSSION .....	36
4.4 CONCLUSIONS.....	41
CHAPTER 5.....	43
INTERFACE HEALING BETWEEN ADJACENT TRACKS IN FUSED FILAMENT	
FABRICATION USING IN-PROCESS LASER HEATING .....	
5.1 INTRODUCTION .....	43
5.2 METHODOLOGY .....	45
5.2.1 LASER PRE-HEATING APPARATUS .....	45

5.2.2 SAMPLE PREPARATION .....	46
5.2.3 MECHANICAL TEST .....	47
5.2.4 TEMPERATURE PROFILE .....	48
5.3 RESULTS AND DISCUSSION .....	48
5.4 CONCLUSIONS.....	55
CHAPTER 6.....	56
IN-PROCESS ROTATING LASER-ASSISTED SURFACE HEALING IN FUSED FILAMENT FABRICATION .....	56
6.1 INTRODUCTION .....	56
6.2 METHODOLOGY .....	58
6.2.1 ROTATING LASER SURFACE HEALING APPARATUS.....	58
6.2.2 THERMAL PROFILE .....	59
6.2.3 SAMPLE PREPARATION .....	60
6.2.4 SURFACE ROUGHNESS.....	62
6.2.5 MECHANICAL TEST .....	62
6.3 RESULTS AND DISCUSSION .....	62
6.3.1 SURFACE ROUGHNESS.....	62
6.3.2 MECHANICAL STRENGTH AND FRACTURE BEHAVIOR .....	66
6.3.3 SURFACE HEALING ON CURVED SURFACE.....	69
6.4 CONCLUSIONS.....	69
CHAPTER 7.....	71

SUMMARY AND CONCLUSIONS .....	71
REFERENCES .....	74
CURRICULUM VITAE.....	82

## LIST OF TABLES

Table 2.1 List of FDM process parameters.....	5
Table 2.2 Ultem 1010 filament specification.....	6
Table 2.3 Specifications of laser parts .....	7
Table 3.1 Specifications of laser parts .....	19
Table 3.2 FFF process parameters .....	20
Table 3.3 PEEK filament specification.....	21
Table 4.1 Laser components specifications .....	32
Table 4.2 PEEK filament specification.....	33
Table 4.3 FFF process parameters .....	33
Table 5.1 Print parameters .....	46

## LIST OF FIGURES

Figure 2.1 Schematic diagram of experimental set for FFF printing using pre-deposition laser heating. ....	8
Figure 2.2 (a) CAD file for single wall rectangular box; (b) G-code for vertical tensile bar milling in Bantam tools software; (c) Machined vertical tensile bar.....	9
Figure 2.3 Tensile strength of laser and control samples.....	9
Figure 2. 4. (a) Cross section of Ultem 1010 filament, (b) Cross section of horizontal control sample break with tensile test; (c) Freeze fracture surface, and (d) tensile test failure surface of vertical control sample (e) Freeze fracture surface and (f) tensile test failure surface of 1.6 W laser sample.....	12
Figure 2.5. Schematic diagram of Reptation and Relaxation, (a) polymer in stretched and disentangled status, (b) reptation only, (c) relaxation only, (d) combination of reptation and relaxation, with entangled arear circled in red. ....	14
Figure 3.1 Schematic diagram of experimental set for FFF printing using pre-deposition laser heating. ....	18
Figure 3. 2. (a) Single wall rectangular box (5 samples each set); (b) Machined tensile bar. ....	20
Figure 3.3 Tensile strength of laser pre-deposition heating PEEK tensile bar and control samples.....	23
Figure 3.4 SEM of tensile test failure surface for (a) Vertical control sample; (b) 2.13 W laser sample. (c) the schematic (side view) of fracture surface progression .....	25



Figure 3.5 Schematic diagram of Reptation and Relaxation(a) Initial state: stretched and disentangled; (b) Relaxation only; (c) Reptation only; (d) Combination of relaxation and reptation. ....	26
Figure 4.1 Schematic diagram of (a) (b) nozzle flow and (c) (d) 90 ° turn. ....	29
Figure 4.2 Schematic diagram of FFF apparatus with pre-deposition laser heating. ....	32
Figure 4. 3 (a) Single wall rectangular box (4 samples each set); (b) Machined tensile bar. ....	34
Figure 4. 4 Tensile strength of laser pre-deposition heating PEEK tensile bar and control samples.....	36
Figure 4. 5 Load-displacement curve for 1.7 W laser pre-deposition heating and control samples.....	37
Figure 4.7 Temperature profile of sample during print. (Cursor is the point where temperature was measured).....	39
Figure 4. 6 SEM of tensile test fracture surface for (a) Control sample; (b) 2.13 W laser sample. ....	38
Figure 4. 8. Schematic diagram of Reptation and Relaxation(a) Initial state: stretched and disentangled; (b) After relaxation: cluster shape, entangled.....	41
Figure 5.1 (a) photo of the laser pre-heating apparatus, (b) schematic diagram of the process.....	45
Figure 5.2 (a) Printed sample and cutting direction of flexural bar. (b) 3-point flexural test .....	47
Figure 5.3 Thermal profile of laser pre-heated spot .....	48
Figure 5.4 Thermal profile of laser pre-heated spot .....	49

Figure 5.5 Displacement before flexural failure or ultimate strength (for samples along track direction).....	51
Figure 5.6 Load-displacement curve of samples in different groups.....	52
Figure 5.7 SEM image of flexural surface at different scales. (a) (c) Control sample, (b) (d) 150 mW laser assisted sample.....	53
Figure 6.1 (a) rotating laser healing apparatus, (b) schematic diagram of the healing process.....	58
Figure 6.3 (a) Printed rectangular box without top and bottom for tensile test (b) milled tensile bars .....	61
Figure 6.4 profilometry data of control (a) and 2.5 mm/s 700 mW laser (c) sample, Optical image of control (b) and 2.5 mm/s 700 mW laser (d) sample from the side (same scale bar).....	63
Figure 6.5 Surface roughness plot .....	64
Figure 6.6 Optical image on top, (a) control, (b) 10mm/s 450 mW, (c) 2.5 mm/s 700 mW (same scale bar for all three of them).....	65
Figure 6.7 Tensile strength of laser treated samples printed at 5mm/s.....	66
Figure 6. 8 SEM image of fracture surface (a) control sample, (b) Laser sample 5mm/s 700 mW. (Same scale bar is used).....	68
Figure 6. 9 Optical image of hose adapters printed .....	69

# CHAPTER 1

## INTRODUCTION

Fused filament fabrication (FFF) has become the preferred method for additive manufacturing of polymers because of its flexibility and cost-effectiveness [1]. The process uses thermoplastic filaments as starting material. The filament is extruded through a heated nozzle, which is maintained above the glass transition temperature of the polymer, and directly deposited to construct a 3D component layer-by-layer [2]. Components with complex shapes can be fabricated easily using slicing software to control process parameters such as density and inner support pattern [3]. Even though FFF has numerous advantages [4] and is capable of printing large number of applicable materials including amorphous polymers like polycarbonate [5], acrylonitrile butadiene styrene [4] and semi-crystalline polymer like poly-lactic acid [6], it suffers from a few drawbacks. For instance, parts fabricated using this method exhibit fairly low mechanical strength compared to those fabricated with traditional methods, particularly in the build direction, and the mechanical properties of FFF-3D printed parts are anisotropic [7].

To address the issue of mechanical property anisotropy in FFF-printed parts, the major thrust in the literature has been to use statistical analysis tools like design of experiments [8–10], Taguchi method [11–14], fuzzy logic [15] and parameter investigation [16,17] to optimize process parameters like nozzle temperature, raster strategy, layer thickness and air gap control [18–22]. The main drawback of these approaches is that they propose a trade-off between different process parameters to achieve maximum inter-layer strength

but do not address the fundamental physics that governs the inter-layer bond formation mechanism. Some other approaches to improving mechanical properties of FFF printed components include printing in vacuum to reduce the porosity and heat losses due to conduction [23], printing in low oxygen environment [24] or using a post-processing thermal treatment [25].

The inter-layer strength of FFF components is dependent on the motion of polymer chains across the interface between layers. This motion of polymer chains, referred to as reptation, is a function of the interface temperature and the time during which the temperature remains above the glass transition temperature of the polymer extrudate [26,27]. To this end, raising print temperature can naturally increase interfacial bond strength due to increase in polymer reptation [28]; however, degradation occurs if temperature exceeds a certain limit [29]. In addition, it is found that weld strength is related to welding time as a function of  $t^{1/4}$  until polymer in the weld region is fully entangled [30–34]. Many studies have been focused on melting behavior of polymer diffusion in equilibrium state [35,36], where it was found that transient behavior of the polymer melt also plays an important role in forming of final microstructure. These factors suggest a potentially effective method to improve mechanical strength with introducing heat directly to the inter-layer interface during printing.

In the past years, several researchers have shown possibility of improving mechanical behavior of FFF built parts along in-plane direction by optimizing process parameters, including layer thickness, width, printing speed [18] printing orientation [19,22], raster angle [20,22], adding support material [21], infill density, shell thickness, and printing temperature [37], statistical analysis tools [8–10] and Taguchi method [11–14]. It can be

found that mechanical strength along in-plane direction exhibits lower mechanical strength as compared to material itself, and that it is a function of print parameters examined in the studies mentioned above. It has been shown that the mechanical strength in in-plane directions of FFF fabricated part can be improved by printing in vacuum to reduce porosity and heat loss due to conduction [23], and a thermal treatment subsequent to process [25]. However, these methods either requires a separate process or a vacuum chamber that can hardly be implemented to most commercial 3D printers. With regard to these approaches, the trade-off between different methods to reach maximum mechanical strength exists as a major drawback, and the fundamental physics dominating the decrease of mechanical strength remain unsolved.

In this work, the effect of laser heating is investigated on the interlayer interface for FFF printed Ultem 10100 and PEEK in Chapter 2 and 3, respectively. The interaction of laser energy along deposited track is researched in Chapter 4. The interface healing between adjacent tracks is investigated in Chapter 5. The surface healing process using laser energy is presented in Chapter 6.

## CHAPTER 2

### AN APPROACH TO IMPROVE INTERFACE HEALING IN FFF-3D PRINTED ULTEM 1010 USING LASER PRE-DEPOSITION HEATING

#### 2.1 INTRODUCTION

In their previous work, authors reported on an in-process laser pre-deposition heating technique with near-infrared laser that was used to heat the interface between current and the previous layers in front of the nozzle to introduce heating directly to the region where reptation is needed. A 77% of increase in bonding toughness (in bending test) compared to that of control samples (samples printed without laser pre-deposition) was reached in FFF-printed ABS material [38,39].

In this work, a similar technique was adapted to use CO<sub>2</sub> infrared laser to assist FFF-3D printing of ULTEM 1010. The tensile strength of horizontal control samples (samples tested along the printed track direction), vertical control sample (samples tested along the build direction), laser pre-deposition heating samples and filament feedstock have been compared. Failures at inter-layer interface and its cross-section have been analyzed. Using these results as well as favorable evidence of improved reptation and entanglement across the interfaces, a scalable approach was developed to build nearly isotropic parts.

#### 2.2 METHODOLOGY

##### 2.2.1 SAMPLE PREPARATION

A high temperature 3D printing platform (Instamsys Funmat HT) was used for pre-deposition laser heating process implementation. The schematic diagram of the setup is shown in Fig. 2.1. A 0.4 mm E3D stainless steel nozzle was used for all samples in this

work. For all prints, 360 °C nozzle temperature, 160 °C bed temperature and 90 °C environment temperature were maintained. Printer motion was controlled by G-codes generated using Instamsys slicing software. Print parameter settings used are shown in Table 2.1.

Table 2.1 List of FDM process parameters

Parameter	Data
Pattern shown in Fig. 2.2 (a)	Single wall
Layer height	0.2mm
Extrusion width	1mm
Extrusion temperature	360 °C
Bed temperature	160 °C
Environment temperature	90 °C
Nozzle speed	10 mm/s
Filament diameter	1.75mm
Raft	Yes

Black Ultem 1010 (PEI Ultem 1010 black, 3DXTech, Grand Rapids, USA) was used to print all testing samples. Material properties of this filament are given by 3DXTech, which are shown in table 2.2. Filament feedstock was placed in an oven at 110 °C over night for dehydration before print, then filament was placed into printer chamber with Uline Silica Gel Desiccants which was also dehydrated overnight. The printing of all samples was performed within 3 hours of removing the filament from the oven and the filaments were replaced in the oven immediately after printing to avoid hydration. Furthermore, the

humidity in the filament chamber was constantly monitored using a monitor (ThermoPro TP50, ThermoPro, Toronto, Canada) to ensure consistent humidity in all print specimens.

Table 2.2 Ultem 1010 filament specification

Parameter	Data
Glass transition temperature	217 °C
Diameter	1.75 mm (+/- 0.05 mm)
Color	Black
Tensile strength	103 MPa
Recommended Extrude Temperature	370 - 390 °C
Recommended Bed temperature	120 - 160 °C
Recommended Print speed	20 – 30 mm/s

A single-wall hollow rectangular box without top and bottom, as shown in Fig. 2.2 (a) was printed layer by layer on raft, with its length along 45 ° to match the direction of laser as shown in Fig 2.1. Laser was turned on and kept at 0 % energy level during raft print for warm-up and then incrementally turned up to the set energy level when sample printing started. After printing, samples were removed immediately from the build plate and then cooled down in air. A wire cutter was used to cut front side, the only side that pre-deposition laser heating occurred, off for tensile bar milling. A desktop PCB milling machine from Bantam tools was used to mill samples into tensile bars, as show in Fig. 2.2 (b). Six tensile bars were acquired from each single-wall box. Shape and size of tensile bars are shown in Fig. 2.2 (c), thickness for all tensile bars were 0.95 mm with negligible variation.



## 2.2.2 LOCALIZED LASER PRE-HEATING APPARATUS

As shown in Fig. 2.1, laser beam was generated by a Synrad laser source. The beam was guided through a coupler, optical fiber (2 meters) and finally was focused to an oval shape spot located 4 mm ahead of the nozzle by a collimator that traveled with the print head (Laser collimator was fixed, so only front wall shown in Figure 2.2 a was pre-heated by laser). Specifications of parts used are shown in Table 3. In this configuration, the surface of existing layer was heated during printing right before material deposition. All laser components used were specifically designed for a laser of 10.6  $\mu\text{m}$  wavelength. The absorption rate of Ultem at 10.6  $\mu\text{m}$  is above 94% [40].

Table 2.3 Specifications of laser parts

Part	Make	Data
Laser source	Synrad 48-1KAN	10.6 $\mu\text{m}$ , 30W max
Coupler	Laser Component	<1dB
Optical fiber	Polymicro	2 meters, < 1dB/meter
Collimator	Laser Component	F=25.4 mm, 19mm
Focused laser	Oval shape	1.5mm*3mm

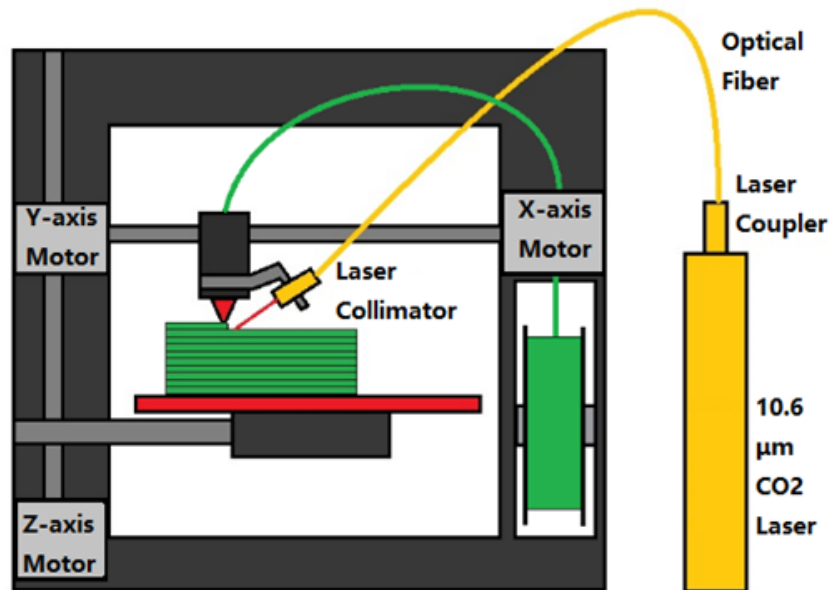


Figure 2.1 Schematic diagram of experimental set for FFF printing using pre-deposition laser heating.

### 2.2.3 MECHANICAL TESTING-TENSILE STRENGTH

A tensile testing machine (MTI-2K, Measurements Technology Inc. Marietta, US) was used to carry out tensile test for all print specimens. 5 samples in each set were examined, the 6th sample in each set was used to remove error samples, such as samples that broke at clip position. Pull speed was set at 3 mm/min for each test specimens. Breaking load (highest load) for all vertical samples, and ultimate tensile strength (highest load in force-deflection curve) for horizontal control samples were used to calculate averages and standard deviations.

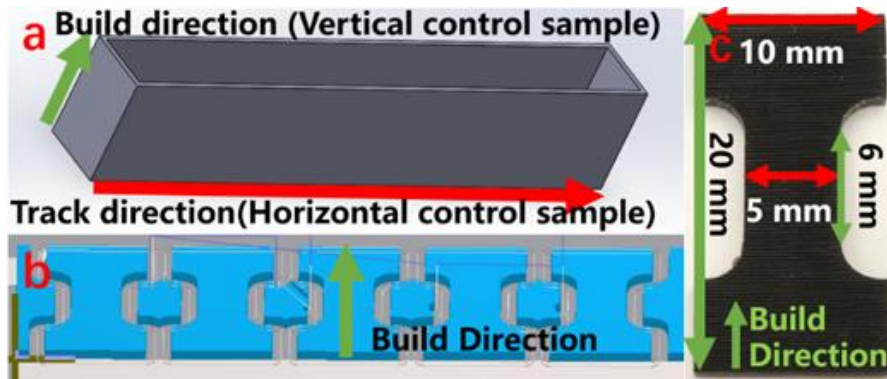


Figure 2.2 (a) CAD file for single wall rectangular box; (b) G-code for vertical tensile bar milling in Bantam tools software; (c) Machined vertical tensile bar..

### 2.3 RESULTS AND DISCUSSION

Due to the nature of rastering of printed tracks in vertical samples, the net areas consisting physical materials are only 92.1%, 76.9% and 85.7% of the nominal areas measured using a caliper for horizontal control, vertical control and laser-assisted samples respectively. These values were used as correction factors. The tensile strength value of horizontal control samples was used as isotropic reference.

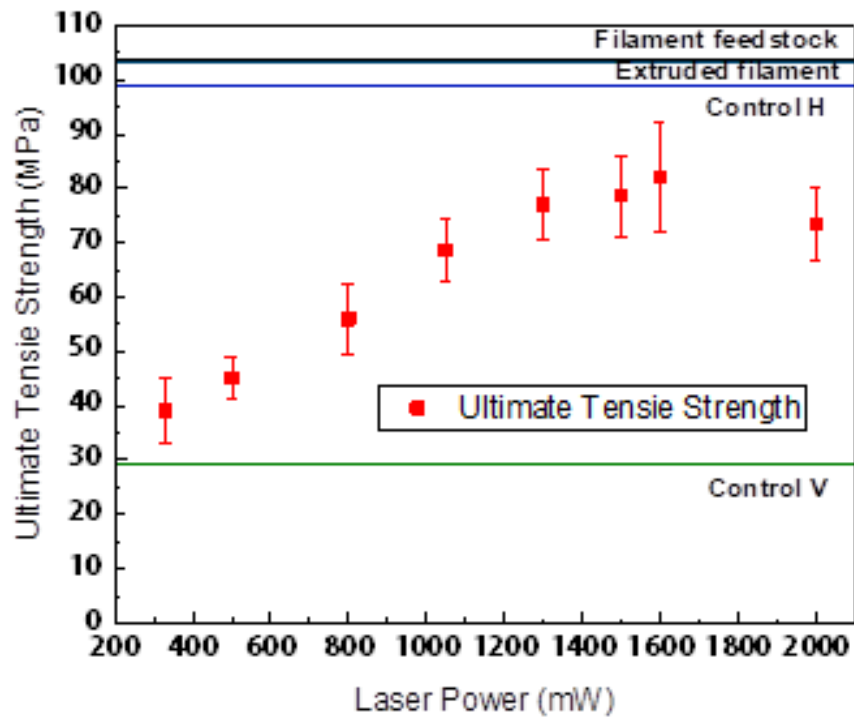


Figure 2.3 Tensile strength of laser and control samples

Tensile strength of laser pre-deposition heating samples and two control samples are shown in Fig. 2.3 where average values and standard deviations are calculated from 5 samples in each set. With laser power ranging from 0.33 W to 2 W, tensile strength of filament feedstock (black line), extruded feedstock (dark green line), vertical control samples (light green line) and horizontal control samples (blue line) are marked as reference lines in the plot for comparison.

Average tensile strength of filament measured by using the tensile tester machine (MTI-2K) was found to be 103.9 MPa, which is in close agreement with the value of 103 MPa provided by the manufacturer. An SEM image of the cross section of the filament after tensile testing is shown in Fig. 2.4 (a). The center part of filament shows a very rough fracture surface while the outer edge shows a relatively smoother fracture surface. This disparate fracture morphology in the center and the edges of the filament can be attributed to the difference in the material flow rate between the center and the edge. During extrusion, to make the printing feedstock, the material flow rate at the center is much higher than that at the edge which is closer to the nozzle walls [41]. This results in the polymer chains at the edge being stretched in the direction of extrusion whereas in the center of the extrudate, the polymer chains remain relatively entangled. Thus at onset of fracture, the breakage of polymer chains at the edge of the sample (which are already aligned in the direction of tensile stress) results in a smoother fracture surface than that of the center, where polymer chain are peeled and pulled-out of entangled chains which results in a rougher fracture morphology. When the filament is further extruded from the 0.4 mm printing nozzle diameter without 90° turn, it showed a slightly lower tensile strength of 103.4 MPa. The authors attribute this drop in strength to the reduction of flow path diameter as the polymer

melt travels through the nozzle, which leads to further stretching and disentanglement in the extruded filament as opposed to the material in the filament feedstock.

As the polymer flows through the nozzle to a printed track on a horizontal surface, a 90 ° turn in the polymer flow is imposed. This transition alone has been predicted to generate greater amount of stretching and disentanglements [41]. However, the analysis in the referred study was based on the condition where the distance between the nozzle and the print surface is greater than the diameter of the extruded filament, and that the extruded filament lays freely on the print surface (or the pervious layer) with only a slight diameter change. In the print conditions used in this study (and most typical print conditions in general), the extruded polymer melt was squeezed in between the nozzle and print surface to form the printed track height. As a result, more stretching and therefore more strain and disentanglement were created, as shown in Fig. 2.5 (a). Furthermore, residual stresses along nozzle travel direction can weaken material in this direction and therefore results in only 95.8% of tensile strength of extruded filament in horizontal control samples. Unlike horizontal control samples, whose tensile strength is based on strength along direction of polymer chain, that of vertical control samples is dominated by inter-layer interface reptation and microstructure around interfaces. It is conceivable that the degree of disentanglement and residual stress increases towards the external surface of the extruded filament (due to nozzle flow and 90 ° turn), which should in turn increase the degree of diffusion due to chain alignment in regions near the interfaces. In most typical prints, however, not enough time at high temperature is allowed for interface healing (re-entanglement and relaxation) to occur. Most polymer chains near interfaces, therefore, show microstructure similar to that represented in Fig. 2.5. (b) (crossed, but not entangled).

Thus, the tensile failure in the vertical samples is expected to occur at the inter-layer interface due to lack of entanglement as shown in Fig. 2.4 (d). As a result, the average tensile strength of vertical control samples was only 29.8% of that in the horizontal control samples without pre-heating.

Laser pre-deposition heating allows higher inter-layer interface temperature, and therefore more reptation and relaxation to happen at the interface, as shown in the conceptual drawing in Fig. 2.5 (d). Additionally, with the increase of laser power, interface temperature increases further, and more reptation and relaxation can take place. This trend continues until it reaches the degradation temperature (510 °C) [42] of Ultem where decomposition and generation of local defect occur.

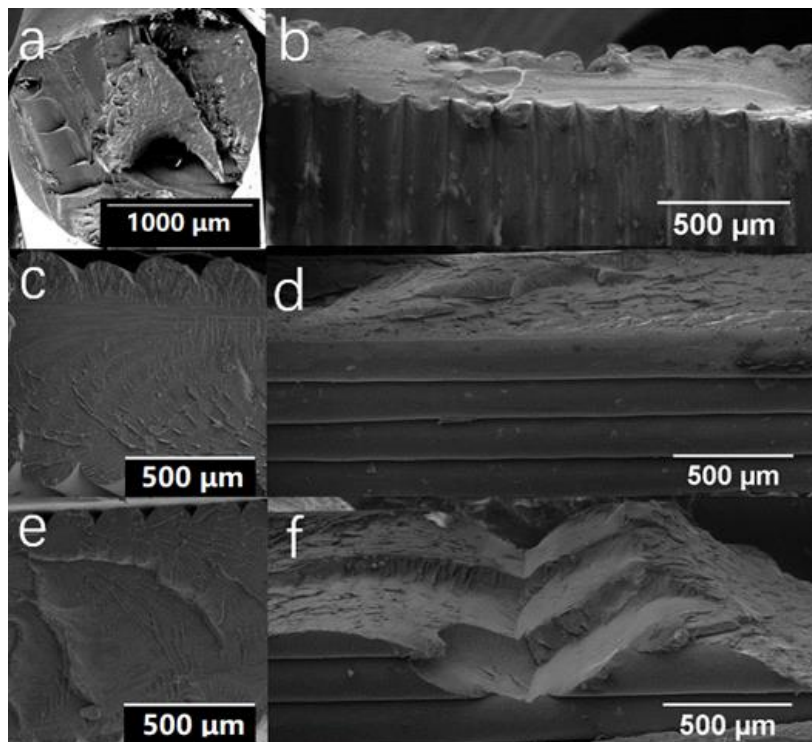


Figure 2. 4. (a) Cross section of Ultem 1010 filament, (b) Cross section of horizontal control sample break with tensile test; (c) Freeze fracture surface, and (d) tensile test failure surface of vertical control sample (e) Freeze fracture surface and (f) tensile test failure surface of 1.6 W laser sample.

As shown in Fig. 2.3, the ultimate tensile strength increased with laser power until 1.6 W, where the average tensile strength reached its maximum value at 82.0 MPa, representing 82.8% of strength of the horizontal control sample, and 278% of that of vertical control sample. The decrease of tensile strength at 2 W is attributed to degradation of polymer since burning and smoke were observed during printing at this power level.

The Scanning Electron Microscopy (SEM) images shown in Fig. 2.4 provide additional insights into the differences in tensile failure. Horizontal control samples shown in Fig. 2.4 (b) exhibited necking during tensile testing. The authors attribute this observation to the nozzle flow and 90° turn that stretches the polymer cluster which induced residual stress. Since the tensile direction is along the direction of polymer chain alignment, the fracture happens due to breakage of polymer chains resulting in a smoother fracture surface.

For vertical control sample shown in Fig. 2.4 (d), the mechanical failure happened along the inter-layer interface; in that, the rough fracture surface morphology also shows evidence of polymer chain peeling and pull-out. This also indicates that the interface healing process has gone through reptation (Fig 2.5. b) at least to some degree. On the other hand, the highly stretched microstructure of polymer chain, as shown in Fig. 2.5 (b), weakens the inter-layer interface bonding. In fact, although enough time was allowed for reptation to occur between layers to reach its theoretical radius of gyration [43], the polymer chains still remained stretched (Fig. 2.5 (b)), and hence the inter-layer interface still represented the weakest region. To improve the tensile strength in vertical samples, longer time is needed for both reptation and relaxation (entanglement) to occur and reach to the state shown in Fig. 2.5 (d).

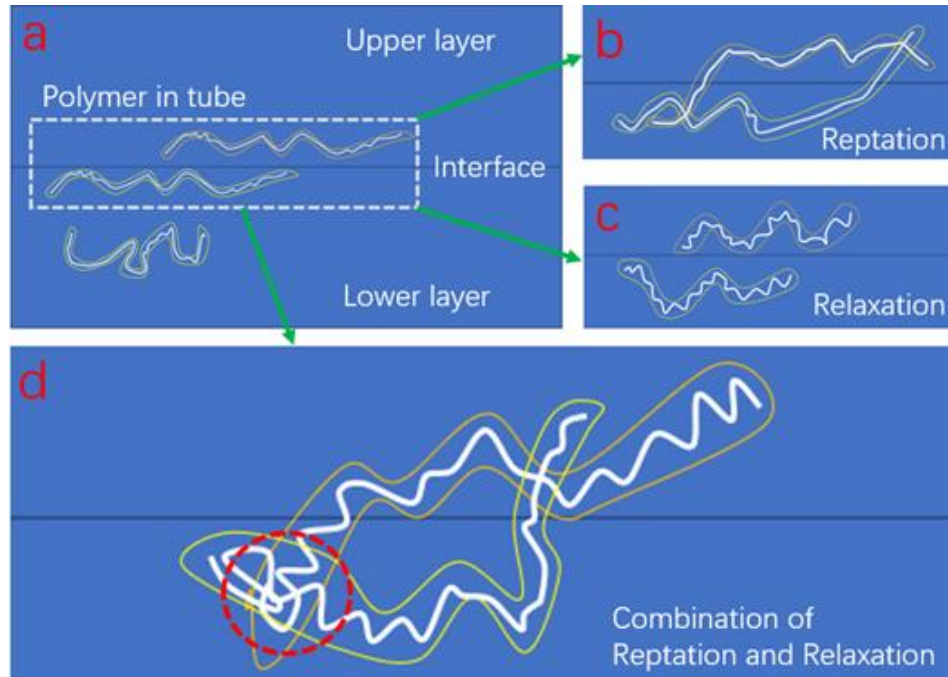


Figure 2.5. Schematic diagram of Reptation and Relaxation, (a) polymer in stretched and disentangled status, (b) reptation only, (c) relaxation only, (d) combination of reptation and relaxation, with entangled area circled in red.

The laser pre-deposition heating sample (at 1.6 W) shown in Fig. 2.4 (f) shows fracture trajectories that extend beyond the boundary of the two adjacent layers with an undistinguishable interface. The sample clearly exhibited behavior resembling isotropic materials. The authors attribute this to the increased temperature and relaxation induced by laser heating which healed the inter-layer interface and the microstructure near interfaces.

The freeze-fracture surfaces of vertical control sample and sample with laser pre-deposition heating can be compared in Fig. 2.4 (c) and (e) respectively. The control samples show a smoother fracture morphology indicating lesser polymer chain reptation and entanglement. The rougher fracture morphology of the samples printed with pre-deposition heating, again, is attributed to higher reptation and entanglement. Since the sample in (b) is broken by pulling but the sample in (c) is broken by freeze fracture, different fracture behaviors and



therefore fracture surfaces geometries and dimensions are expected. Overall, the samples printed with pre-deposition heating exhibited rougher surface morphology. The authors attribute this behavior to the increased temperature-dependent relaxation, which consequently entangled polymer chains and relaxed residual stresses generated through the nozzle flow and 90° turn.

## 2.4 CONCLUSIONS

In the work presented here, the effect of pre-deposition laser heating process using 10.6  $\mu\text{m}$  laser from 0.33 W to 2 W on the tensile strength and fracture behavior of FFF-printed Ultem 1010 have been investigated. Tensile strength of printed parts in the build direction increased with laser power up to 1.6 W, and reaches 82.8% of that in the print direction (horizontal control sample); equivalent to 178% increase in strength in build direction compared to those in the control samples. This strong inter-layer bonding emerged as a result of increased temperature and time dependent relaxation. It is hypothesized with indirect evidence that the increase in inter-layer strength is due to healing of the interface as a result of higher reptation and entanglement of polymer chains at presence of laser pre-deposition heating. The results markedly highlight the laser pre-deposition heating as a feasible approach to improve the built-part isotropy for the extrusion-based polymer 3D printing processes.

## CHAPTER 3

### EFFECT OF IN-PROCESS LASER INTERFACE HEATING ON STRENGTH ISOTROPY OF EXTRUSION-BASED ADDITIVELY MANUFACTURED PEEK

#### 3.1 INTRODUCTION

The Fused filament fabrication (FFF) has turned out to be one of the desired method for thermal plastic additive manufacturing due to its flexibility, capability and cost-effectiveness [1]. Thermoplastic filaments are taken as the starting material during the process. After being extruded through a heated nozzle, the filament is kept nearly above the glass transition temperature of the thermoplastic polymer filament. Then, it undergoes the process of direct deposition and layer-by-layer construction of a 3D component [2]. Utilizing a slicing software to control process parameters such as density and inner support pattern, the fabrication of components with complex shapes can be easily achieved [3]. Despite multitude of advantages [4] as well as the capability to print various applicable materials; i.e. amorphous polymers like acrylonitrile butadiene styrene [4], polycarbonate [5] and semi-crystalline polymer like poly-lactic acid [6], FFF still suffers from several shortcomings. For instance, the parts fabricated by this method possess poor mechanical strength, especially in the build direction, in contrast to those manufactured with traditional methods. Moreover, the mechanical properties exhibited by FFF-3D printed parts are anisotropic [7].

In order for resolving the mechanical property anisotropy in FFF-printed parts, optimizing process parameters (such as nozzle temperature, layer thickness, raster strategy and air gap), ultrasound based techniques [18–22,44] and use of statistical analysis tools (design of

experiments [8–10], Taguchi method [11–14], fuzzy logic [15] and parameter investigation [16,17]) have been the major thrust in the literature. With regard to these approaches, the current major shortcoming is a trade-off between different process parameters for the purpose of reaching the maximum inter-layer strength. However, the fundamental physics governing the inter-layer bond formation mechanism remain unresolved. According to some other methods, the mechanical properties possessed by FFF printed components could be improved by; for instance, printing in vacuum to mitigate the heat losses and porosity induced by conduction [23], ultrasound-assisted printing [44], printing in low oxygen environment [24] or carrying out thermal treatment subsequent to processing [25]. Previously, an in-process laser pre-deposition heating technique with near-infrared laser was reported for heating of the interface between current and the previous layers ahead of nozzle path. In comparison to control samples (samples printed without laser pre-deposition), the bonding strength (in bending test) was improved by 77% in FFF-printed ABS material [38,39]. The work was further improved to reach 83% tensile strength of that along in-plane direction, using a 10.6  $\mu\text{m}$  infrared  $\text{CO}_2$  laser with Ultem 1010 [45].

In this study, to facilitate FFF-3D printing of PEEK by  $\text{CO}_2$  infrared laser, a redesigned and optimized technique was applied. A comparison is performed with tensile strength of horizontal control samples (samples tested along the printed track direction), vertical control sample (samples tested perpendicular to track direction), laser pre-deposition heating samples and filament feedstock. In addition, an analysis is presented to probe failures at inter-layer interface as well as over cross-section. A scalable approach was devised to produce nearly isotropic parts by using these results along with supporting evidence of improved reptation and entanglement across the interfaces.

## 3.2 METHODOLOGY

### 3.2.1 LOCALIZED LASER PRE-HEATING APPARATUS

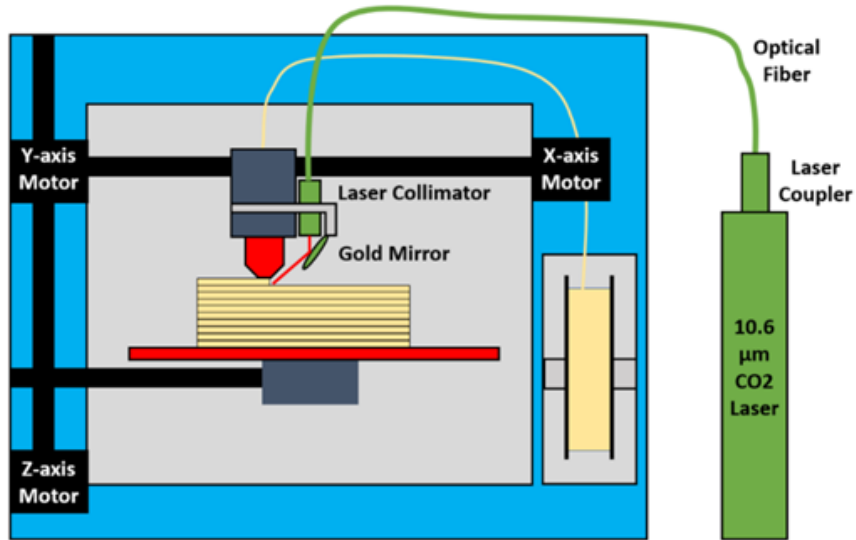


Figure 3.1 Schematic diagram of experimental set for FFF printing using pre-deposition laser heating.

A high temperature printing system with laser pre-deposition heating process was built with a closed-chamber 3D printer (Funmat HT, Intamsys, Shanghai, China) along with the laser components. As shown in Fig. 3.1, first, a laser beam was generated by a 10.6 μm CO<sub>2</sub> Laser. This beam then was coupled by a laser coupler into an optical fiber which was focused by a laser collimator to a spot-reflected using a gold mirror at a 2 mm distance away (edge of beam to edge of nozzle) from nozzle on the previously printed layer. Specifications of optical parts used are shown in Table 1. The focused beam spot was oval-shaped with a size of 4 mm and 2.5 mm in length and width, respectively. The laser collimator and gold mirror were held by a bracket that was installed on the extruder, allowing the laser spot to travel with the extruder and to stay focused on the previously printed layer while the extruder moves from left to the right. The bracket is designed to hold 4 laser collimators and 4 gold mirrors along 4 directions in x-y plane (+x, -x, +y, -y).

In this work, laser along +x direction is used for all the prints. It is worth noting that since laser collimator was installed and held vertically in the new design, the loss of printable area due to additional laser apparatus significantly reduced compared to that in previous setting [45].

Table 3.1 Specifications of laser parts

Component	Make/Shape	Specifications
Laser Source	Synrad 48-1KAN (Mukilteo, USA)	Wavelength:10.6 $\mu\text{m}$ , Power: 30W max
Coupler	Laser Component (Bedford, USA)	Energy loss <1dB
Optical fiber	Polymicro (Phoenix, USA)	Length: 2 meters, < 1dB/meter
Collimator	Laser Component (Bedford USA)	Focal Length:25.4 mm, Diameter:19mm
Focused laser	Elliptical	Size: 4mm*2.5mm

### 3.2.2 SAMPLE PREPARATION

All prints were fabricated using high temperature 3D printing system with laser pre-deposition heating introduced above. There are two categories of samples prepared, control and laser samples, prepared without and with laser pre-deposition heating, respectively. The tensile strengths of laser samples (z-direction, for inter-layer strength) were compared to that of control samples along both build direction (z-direction, for inter-layer strength,

vertical control sample) and in-plane direction (x-direction, for inner-layer strength, horizontal control sample).

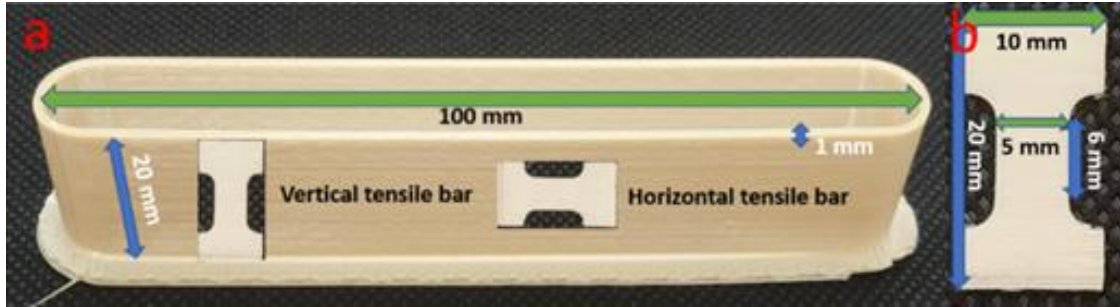


Figure 3. 2. (a) Single wall rectangular box (5 samples each set); (b) Machined tensile bar.

The printer is controlled by G-codes generated in Intamsys slicing software. A 0.4 mm (that is commonly used in commercial 3D printer) E3D stainless steel volcano nozzle was used for all prints in this work. 380 °C nozzle temperature, 150 °C build plate temperature, and 90 °C ambient temperature were maintained for all builds based on manufacture recommendations and parameter space investigation. Other process parameters were shown in Table 2. Homogeneous PEEK (3DXTech, Grand Rapids, USA) was used as the filament feedstock. Filament specification given by 3DXTech is shown in Table 3. In order to avoid the influence of humidity, the filament was kept in a furnace at 100 °C for dehydration overnight. Before printing, Uline silica gel desiccant was used to maintain low humidity in filament chamber during print and a hygrometer (Thermo Pro TP50, Thermo, Toronto, Canada) was used to ensure consistent low humidity being maintained inside the chamber for all prints.

Table 3.2 FFF process parameters

Parameter	Data
Pattern shown in Fig. 3.2 (a)	Single wall

Layer height	0.2mm
Extrusion width	1mm
Extrusion temperature	380 °C
Bed temperature	150 °C
Environment temperature	80 °C
Print speed	10 mm/s
Raft	Yes

Table 3.3 PEEK filament specification

Specification	Data
Glass transition temperature	143 °C
Diameter	1.75 mm (+/- 0.05 mm)
Density	1.3 g/cc
Color	Natural/Tan
Tensile strength	100 MPa
Recommended Extrude Temperature	375 - 410 °C
Recommended Bed temperature	130 - 145 °C
Recommended Print speed	10 – 50 mm/s

The part printed was a single-wall hollow rectangular box, 100 mm long, 13 mm wide and 20 mm-tall with two semi-circular ends is shown in Fig.3.2 (a). A raft was used for the base. The longer side of the box was along x-axis to match the direction of laser focused spot as shown in Fig. 3.1. During raft print, laser was turned on and maintained at 0% output power for warmup, then gradually increased using power knob to the final power level (in percentage of laser power) when raft was finished. The output power was measured using a Power meter (Thorlabs, Newton, US). The box was printed layer by layer

with a 0.2 mm layer height and 1 mm width. It is important to notice that only front side of the box, where nozzle moves from left to right, was pre-deposition heated while the backside of the wall was post-deposition heated. After print, the box was removed from build plate immediately and cooled down to the room temperature outside the chamber.

A rotary cutter (Dremel, Mount Prospect, US) with 0.5 mm thick diamond wheel was used to cut the rectangular box into flat wall shapes to be used in milling machine, since printed PEEK was too brittle to be cut using wire cutter. Only the front side (where pre-deposition heating occurred) was used for tests. A desktop PCB milling machine was used to mill samples into tensile bars. Seven tensile bars can be milled out from each cut wall. Shape and size of one sample tensile bar is shown in Fig.3.2 (b).

### 3.2.3 MECHANICAL TESTING-TENSILE STRENGTH

MTI-2K tensile testing machine (Measurements Technology Inc. Marietta, US) was used to test PEEK tensile bars. Out of seven samples cuts from left to right, the 5 middle tensile bars machined from each set were used for testing and the last two tensile bars in each set were used as replacement of error data, i.e. samples that broke by metal clip on tensile tester. A pre-load of 3 N was used and pulling speed was set to be 5 mm/s. Ultimate tensile strength was used as reference for all tensile bars.

### 3.3 RESULTS AND DISCUSSION

Tensile strength data of laser pre-deposition heating PEEK samples (along the build direction, red dots), horizontal control samples (Control H), and vertical control samples (Control V) are shown in Fig. 3.3. The average (red dot) and standard deviation (error bar) were calculated from 5 samples in each set. The straight line for horizontal control sample



and vertical control sample are averages of 5 samples as well. From Fig. 3.3, laser pre-deposition heating increased inter-layer bonding strength by a factor greater than 4 (increase of 350%), from 17.8 MPa to 80.4 MPa at 2.13 W of laser power. Of particular interest, the laser sample (at 2.13 W) shows 99.5% tensile strength compared to that of horizontal control sample with the standard deviation of 3.7%. Along with this investigation, the SEM image also revealed further details of fracture propagation at tensile test as shown in Fig. 3.4 (b). It is evident from these images that the fracture surfaces in laser samples extend inside layers, while fracture surface of vertical control samples stopped at the layer interface and did not progress inside the layers. Thus, it can be confidently concluded that the laser pre-deposition heating has increased the bonding strength at the interface to as strong as the material strength (strength of extruded filament feedstock).

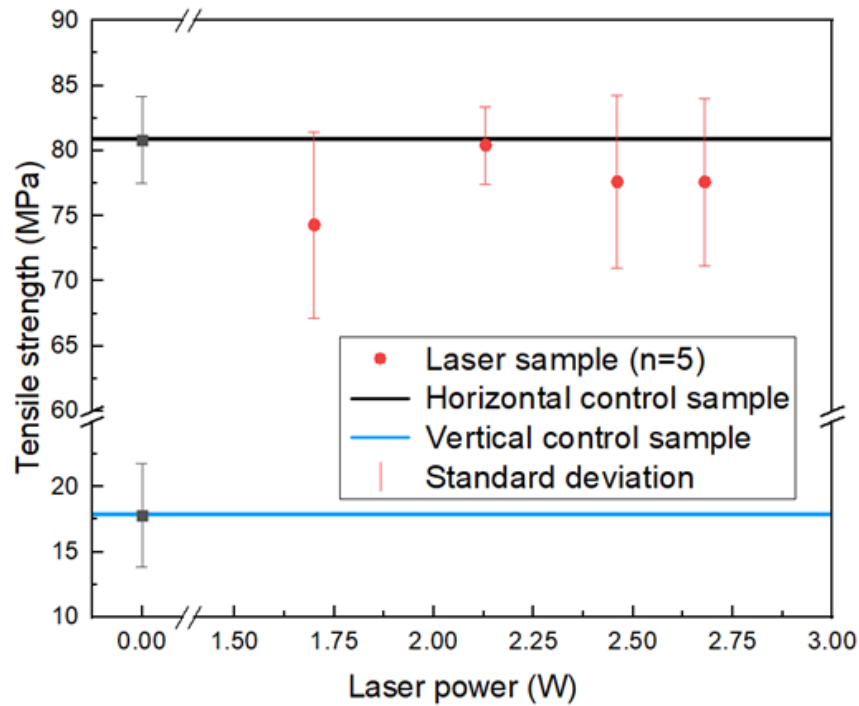


Figure 3.3 Tensile strength of laser pre-deposition heating PEEK tensile bar and control samples.

Note that tensile strengths for vertical control samples, horizontal control samples and 3DXTech data (shown in Tab. 3) are 17.8 MPa, 80.8 MPa and 100 MPa, respectively. Hence, there has been 19.2% tensile strength loss with respect to original material through the printed track. This strength loss is highly likely caused by shear flow in the nozzle, which elaborated in rheological model in [41]. Briefly, in this model, shear force applied to polymer within the nozzle is a function of flow rate and distance from the nozzle wall. The nozzle shear force, in essence, induces stretch and disentanglement to polymer chains, which ultimately give rise a reduction in mechanical strength of the material.

In order to increase inter-layer reptation, laser pre-deposition heating was used to increase the interface temperature, which expected to increase reptation and relaxation at the inter-layer interface as shown in the conceptual drawing in Fig. 3.5. The relationship between the interlayer strength and the mass transfer and microstructure of polymer can be described by the relationship proposed by Ezekoye [34].

$$\frac{\sigma_t}{\sigma_{max}} = \left( \frac{t_{weld}}{\tau_{rep}} \right)^{1/4} = \left( \frac{t_{weld} D_s}{R_g^2} \right)^{1/4} \quad (3.1)$$

where  $\sigma_t$ ,  $\sigma_{max}$  are the strength of the interface and the tensile strength of the material respectively,  $t_{weld}$  is the healing time of the interface (or time during which the interface stays above glass transition or melting temperature),  $\tau_{rep}$  is the reptation time,  $D_s$  is the center of mass diffusivity of polymer chains, and  $R_g$  is the radius of gyration of polymer chains.

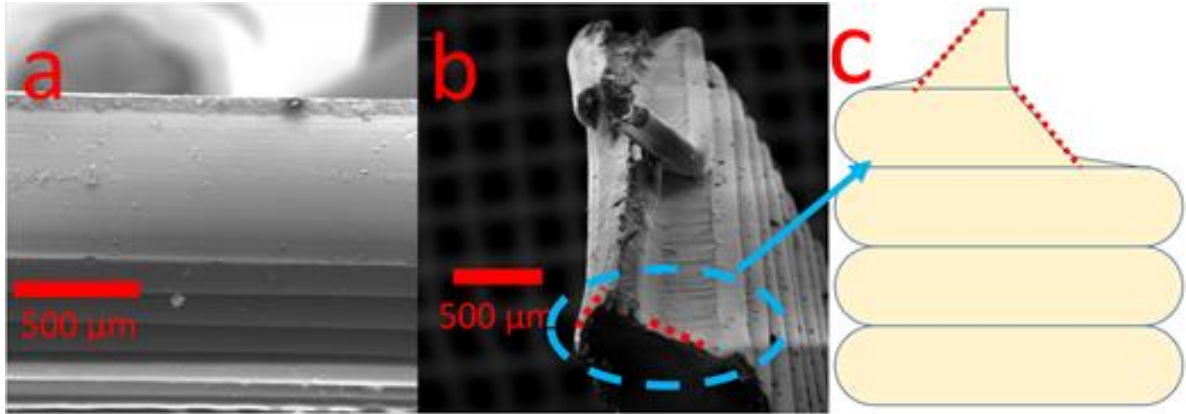


Figure 3.4 SEM of tensile test failure surface for (a) Vertical control sample; (b) 2.13 W laser sample. (c) the schematic (side view) of fracture surface progression

In this work, it is hypothesized that laser was used to increase interface temperature yet below the threshold of degradation limit, which is expected to give rise longer reptation time to reach a high percentage of isotropic microstructure. As a result, tensile strength of laser pre-deposition heating sample reached 99.5% that of horizontal control sample (breaking polymer chains). As shown in Fig.3.4 (b), the fracture trajectory starts from the edge and breaks into layer and ends up with a curved surface that extends to an upper layer at the center. Parts of this behavior may be attributed to the fact that the longer edge of the track was exposed to air, hence cooled down faster than that in the center, i.e. allowing less time for relaxation and reptation. As the crack edge moves from the side interface towards center, it fairly shows a 45-degree inclination, perhaps due to ductile fracture in shear mode.

The average tensile strength increased with laser power until the degradation temperature was reached (575 - 580 °C) [46]. As shown in Fig. 3.3, the tensile strength of PEEK laser sample increased until 2.13 W, after which it began to decline in the range between 2.13 W and 2.97 W due to polymer degradation.

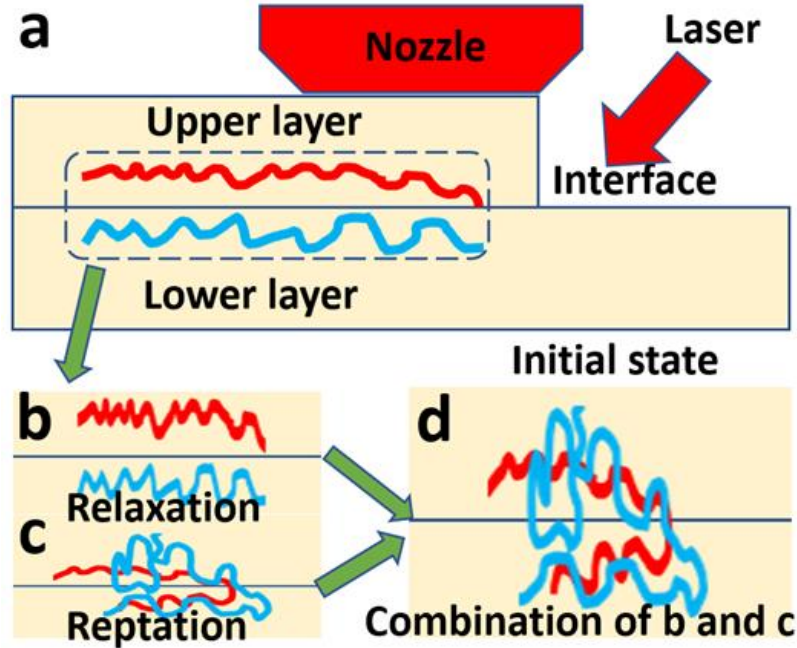


Figure 3.5 Schematic diagram of Reptation and Relaxation (a) Initial state: stretched and disentangled; (b) Relaxation only; (c) Reptation only; (d) Combination of relaxation and reptation.

It is hypothesized that nearly all polymer chains are highly stretched and disentangled. Thus, in order for the printed polymer to recover to isotropic status, the polymer chains need to recover from the residual stresses induced by nozzle flow and 90 ° turn, and reptate as far as the radius of gyration. The conceptual drawing of initial state is shown in Fig. 3.5 (a), where the red curve represents a polymer chain at bottom of upper layer, and the blue curve represents a polymer chain at top of lower layer. Both polymer chains are highly stretched (not in cluster shape). The polymer relaxation and reptation are two of key elements playing role in constructing interlayer adhesion independently, despite both are

function of temperature. Through relaxation, the polymer chains tend to undergo a spring back to its original length with subsequent reduction of residual stress (Fig. 3.5 (b)). The reptation however is tendency of the polymer chains to slide along with a possibility of crossing the inter-layer interface to entangle with polymer chains in the other layer. The driving force for reptation is thermal diffusion and chain geometry ( $D_s$ ,  $R_g$ ) while that for the relaxation is rheology, i.e. polymer viscoelastic properties. Previous studies [43] found out sufficient time above glass transition temperature needs to be given in order to obtain isotropic property in regular 3D printing parts (as predicted in Equation above). This outcome however will not fully occur in reality, possibly due to missing effect of relaxation and entanglement in as other factors affecting in forming interlayer adhesion.

### 3.4 CONCLUSIONS

This work presents the effect of laser pre-deposition heating on tensile strength and tensile fracture behavior of FFF-printed PEEK. Tensile strength of laser pre-heated sample at 2.13 W reaches 80.4 MPa, which is 99.5% of that in in-plane direction, equivalent to 350.9% increase compared to control sample along build direction. The higher temperature exposure of layer interface and increased time dependent relaxation led to a marked increase in inter-layer bonding strength. Based on indirect evidence, it was speculated that the rising level of inter-layer strength can be attributed to the healing of the interface, which is driven by increased reptation and entanglement of polymer chains under the context of laser pre-deposition heating. Based on these results, laser pre-deposition heating is considered as a viable means of improving the built-part isotropy and their mechanical strength to enhance the extrusion-based polymer 3D printing processes.

## CHAPTER 4

### RELAXATION OF RESIDUAL STRESS IN FUSED FILAMENT FABRICATION PART WITH IN-PROCESS LASER HEATING

#### 4.1 INTRODUCTION

The fused filament fabrication (FFF), which uses thermoplastic filament as raw material to produce 3D objects, has become a desired method for additive manufacturing because of its capability of complex shape and affordable cost [1]. While traditional methods for thermal plastic polymer such as injection molding, blow molding, and thermoforming requires a mold before fabrication. In FFF process, a filament of thermoplastic material is pushed into a hot extruder that stays above the glass transition temperature, driven by a stepper motor roller. At the bottom of the extruder head, where a nozzle is installed, the molten filament is extruded and directly deposited on top of build plate or previously printed layer. With the 3-axis motion, a 3D component can be constructed layer by layer using this technique [2]. In order to build a 3D component, a slicing software is used to slice the part file into layers for fabrication, as well as to control movement of 3-axis, extrusion, and other process parameters, so that a complex part can be easily fabricated [3]. Although FFF process exhibits multiple advantages [4], as well as the capability of fabrication using various thermal plastic materials including soft material like polyurethane (TPU) [47], amorphous polymers like acrylonitrile butadiene styrene (ABS) [4], polycarbonate (PC) [5], and semi-crystalline polymer like Nylon [48] and poly-lactic acid (PLA) [6], it still suffers from several drawbacks. For example, parts fabricated using this method exhibit low mechanical strength compared to that made using traditional methods [7,49].

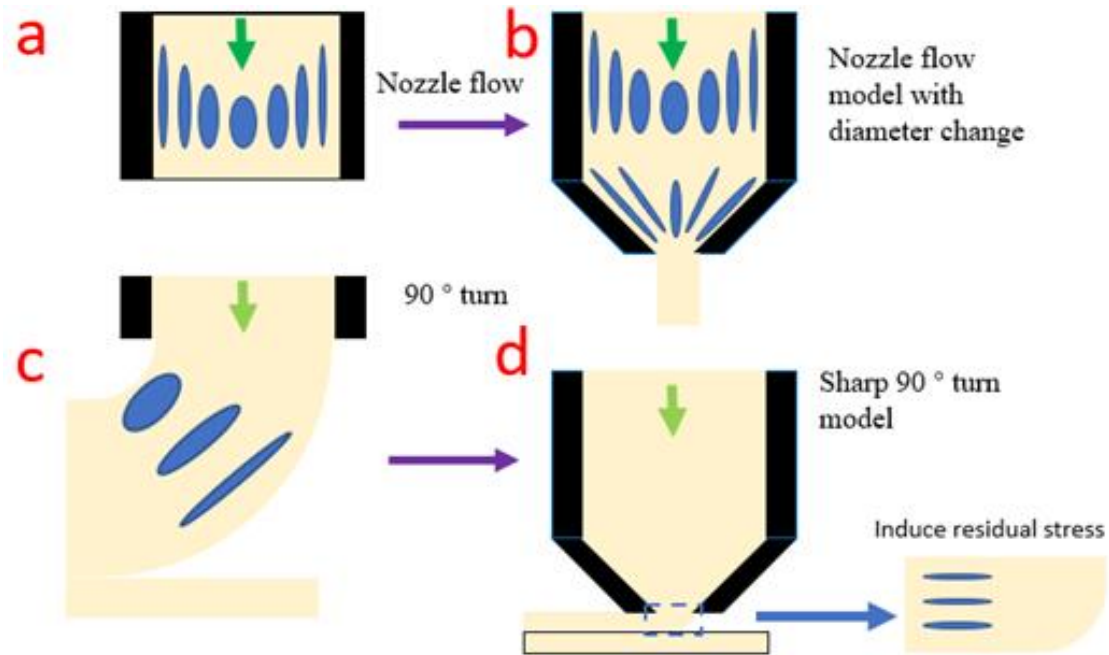


Figure 4.1 Schematic diagram of (a) (b) nozzle flow and (c) (d) 90 ° turn.

The fundamental physics was explained by two models built for nozzle flow and 90° turn in extrusion-based additive manufacturing [41] as shown in Fig. 4.1. In the nozzle flow model, while molten filament flows inside a nozzle, a shear flow is generated due to the friction between molten filament and nozzle wall, which increasingly stretches the polymer chain as it moves closer to nozzle wall as shown in Fig. 4.1 (a). In reality, the inner diameter of nozzle from a commercial 3D printer usually decreased from 1.75 mm to 0.4 mm, which significantly increased the shear flow velocity, which therefore, stretches polymer chains in filament to a larger extent as described in Fig. 4.1 (b). The 90° turn model presents the material flow during the deposition process that the molten polymer flow turns from vertical direction in the nozzle to be horizontally deposited track on a build plate or previous layer. During this process, upper and lower sides of the deposited polymer track exhibit compression and tension, respectively as shown in Fig. 4.1 (c). However, the model is based on an ideal situation where filament flows freely in air before touches on a surface.

In reality, in order to achieve a decent strength and Z-resolution, a commonly used layer thickness is 0.1 or 0.2 mm, which is only half or a quarter of the nozzle diameter. So, disentanglement and stretch are likely to happen along the entire thickness as shown in Fig. 4.1 (d). As a result, due to the combination of nozzle flow and 90° turn, residual stresses are induced to the printed part, therefore weakens the mechanical strength.

In order to reduce residual stress, a thermal process is required to heat polymers up to a more motive status. For linear polymers, it is assumed that polymer chain is confined in a tube region (reptation theory), where stress can relax by diffusing curvilinearly [50]. The stress relaxation modulus  $G(t)$  shows high value in short time and decreases exponentially at longer time when it reptates away from its tube [50]. Reptation enhance the relaxation of residual stress at short time in longitudinal modes due to the redistribution of polymer in the tube after deformation [51]. The stress relaxation modulus is shown below for residual stress relaxation [51]. Note that only first term for residual stress was shown in the equation, second term and third term for longitudinal relaxation and Rouse relaxation, respectively were not included.

$$G(t) = 0.8G_e\mu(t)R(t) \quad \text{Equation 4.1}$$

With  $G_e = \rho RT/M_e$  ( $M_e$  is the entanglement molar mass,  $\rho$  is the density,  $T$  is the absolute temperature and  $R$  is the ideal gas constant) being the entanglement modulus.  $\mu(t)$  is the single chain relaxation function,  $R(t)$  is the relaxation function due to constraint release.

Previously, research on inter-layer bonding strength with in-process laser pre-deposition heating technique has been working on since 2016 [38,39,44,45,52]. With optimization of the process over years, the tensile strength of printed part along build direction has finally



reached 99.5% isotropic (compare to control sample along in-plane direction) [52]. However, it has been found that the tensile strength value of control sample tested along in-plane direction lies below that of the material itself due to the mechanism of extrusion-based additive manufacturing process.

In this work, the research was focused on the effect of laser pre-deposition heating on strength along in-plane direction. A comparison is performed with tensile strength of control samples, laser samples along in-plane direction and the bulk material itself. In addition, mechanical behavior including fracture and elongation were analyzed, and hypothesized possible effect of laser pre-deposition heating on microstructure. A scalable method was designed to fabricate parts with less residual stress. Note that the residual stress was inevitable due to the mechanism of extrusion-based additive manufacturing process.

## 4.2 MATERIALS AND METHODS

### 4.2.1 LASER PRE-HEATING APPARATUS

The printer was constructed with a commercial high-temperature 3D printer (Funmat HT, Intamsys, Shanghai, China) and laser components. As shown in Fig. 4.2, the 10.6  $\mu\text{m}$  laser source was located outside of the printer chamber. The beam generated by laser source was then coupled with a laser coupler at one end of an optical fiber. Next, the laser was guided by the optical fiber into the printer chamber with the other end connected to a laser collimator that installed vertically on one side of the extruder. The laser beam was finally focused by the laser collimator on the previous laser with a mirror that is installed on extruder. The focused laser spot (oval shape) locates 2 mm ahead of nozzle on the right side (2mm is measured from edge of nozzle to edge of laser spot). The focused laser spot was 4 mm long and 2.5 mm wide. All specifications of optical components above are

shown in Table. 1. To hold the laser collimator and gold mirror on to the extruder, a custom bracket was 3D printed with Ni Fe alloy as replacement of original hot end. This bracket was designed to hold lower end of heatbreak, volcano nozzle, heater, thermistor, 4 laser collimators and 4 gold mirrors along 4 directions in x-y plane (+x, -x, +y, -y, but only the direction used in this work was connected to optical fiber as shown in Fig.4.2). In this particular work, collimator and gold mirror along +x direction was used for all the prints.

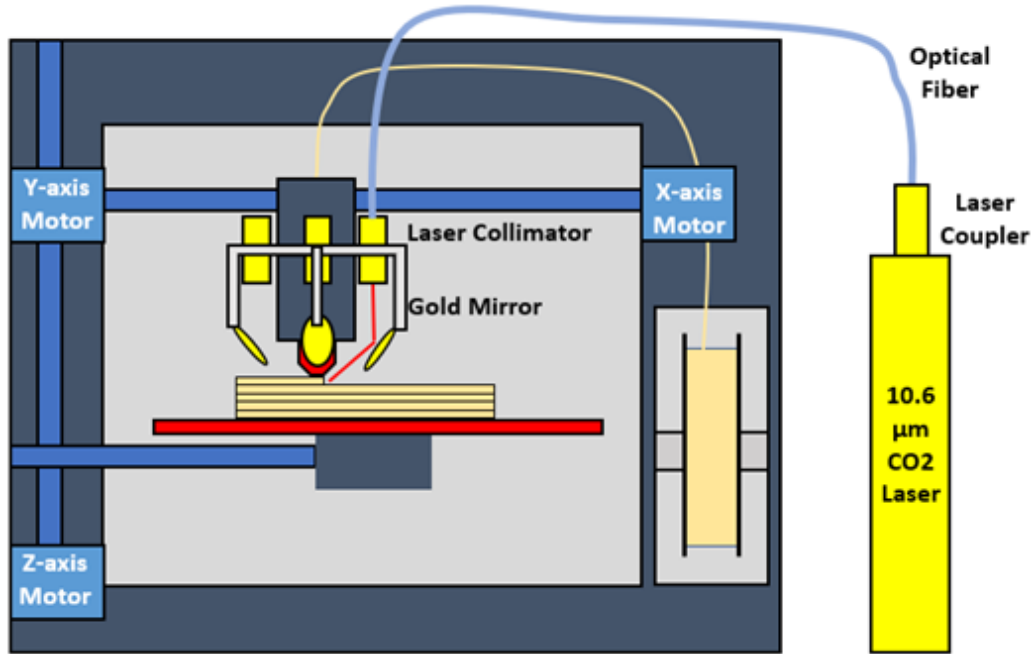


Figure 4.2 Schematic diagram of FFF apparatus with pre-deposition laser heating.

Table 4.1 Laser components specifications

Component	Make/Shape	Specifications
Laser Source	Synrad 48-1KAN (Mukilteo, USA)	Wavelength: 10.6 μm, Power: 30W max
Coupler	Laser Component (Bedford, USA)	Energy loss <1dB
Optical fiber	Polymicro	Length: 2 meters, < 1dB/meter

	(Phoenix, USA)	
Collimator	Laser Component (Bedford USA)	Focal Length:25.4 mm, Diameter:19mm
Focused laser	Elliptical	Size: 4mm*2.5mm

#### 4.2.2 SAMPLE PREPARATION

Homogeneous PEEK filament (3DXTech, Grand Rapids, USA) was used in this work. Filament specifications is shown in Table. 2 and printing process parameters is shown in Table. 3. Based on the recommendation of filament manufacturer, the filament was kept in an oven at 100 °C for dehydration overnight prior to printing. During printing, the filament was placed in a closed filament chamber with silica gel desiccant (Uline, Pleasant Prairie, US) and a hygrometer (TP 50, Thermo Pro, Toronto, Canada) to maintain and ensure consistent low humidity.

Table 4.2 PEEK filament specification

Specification	Data
Glass transition temperature	143 °C
Diameter	1.75 mm (+/- 0.05 mm)
Density	1.3 g/cc
Color	Natural/Tan
Tensile strength	100 MPa
Recommended Extrude Temperature	375 - 410 °C
Recommended Bed temperature	130 - 145 °C
Recommended Print speed	10 – 50 mm/s

Table 4.3 FFF process parameters

Parameter	Data
Pattern shown in Fig. 4.3 (a)	Single wall
Layer height	0.2mm
Extrusion width	1mm
Extrusion temperature	380 °C
Bed temperature	150 °C
Environment temperature	80 °C
Print speed	10 mm/s
Raft	Yes

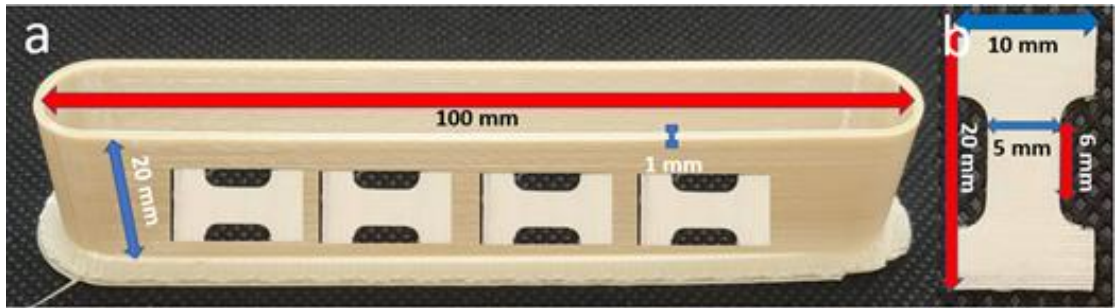


Figure 4. 3 (a) Single wall rectangular box (4 samples each set); (b) Machined tensile bar.

The raw sample printed was hollow closed-cycle box with a single-track wall as shown in Fig. 4.3 (a). This part was 100 mm long, 13 mm wide and 20 mm tall with two straight long sides and two semi-circular ends. The thickness of wall was 1 mm. To increase adhesion with build plate, raft was added to the print setting. For samples with laser pre-deposition heating, the laser source was turned on and kept at 0% power output during raft printing, then it was gradually increased with a power knob to the targeted power level within 5 seconds before the end of raft printing. It is worth noting that only when the nozzle was moving from left to right (which is the front side in this work), the laser spot would be in front of nozzle, therefore, pre-deposition laser heating treatment. After print session, the

sample was taken out from printer chamber immediately and allowed to cool down to room temperature.

In order to cut the front side of the part into feasible shape for milling machine, a rotary cutting tool (Dremel, Mount Prospect, US) equipped with a half millimeter thickness diamond wheel was used. To mill the front side wall into tensile bars for tensile test, a desktop milling machine (Bantam tools, Peekskill, US) was used. From each front wall, 4 tensile bars can be machined out. The dimensions of the tensile bar are shown in Fig. 4.3 (b).

#### 4.2.3 MECHANICAL TEST

Tensile test was done on PEEK tensile bars prepared above. The test station used was MTI-2K tensile testing machine (Measurement Technology Inc. Marietta, US). In each group, 4 tensile bars were used for tensile test. During tensile testing, the pre-load applied was 3 N and the pulling rate was 5 mm/s. The ultimate tensile strength was used for all PEEK tensile bars as recommended in the reference.

#### 4.2.4 TEMPERATURE PROFILE

A FLIR a6753sc thermal camera (FLIR, Wilsonville, US) was used to acquire the temperature profile of laser heated surface from an orthogonal view. The middle pixel along the build direction of the laser heated/control layer was used to represent the temperature of the layer. The frequency of the recording is 60 frames per second.

### 4.3 RESULTS AND DISCUSSION

Tensile test data of the PEEK samples through the pre-deposition laser heating process are shown in Fig. 4.4. The average and standard deviation calculated from 4 samples in each set were illustrated as red dot and red error bar, respectively. The straight line at 83.9 MPa was used as a reference for the tensile strength of control sample without laser pre-deposition heating. As is evident in Fig.4.4, while all laser samples showed similar behavior for tensile strength with no detectable trend, all of their strength values fall well above those for control sample. With the effect of laser pre-deposition heating process, the tensile strength was increased to 93.5MPa at 1.7W of laser power, which represents 11.4% increase compared to control sample. Moreover, not only did this laser process enhanced the part's strength, but also greatly increased its elongation prior to fracture as shown in Fig.4.5. Thus, it can be inferred that the laser pre-deposition techniques also play a key role in altering the fracture behavior in tensile test.

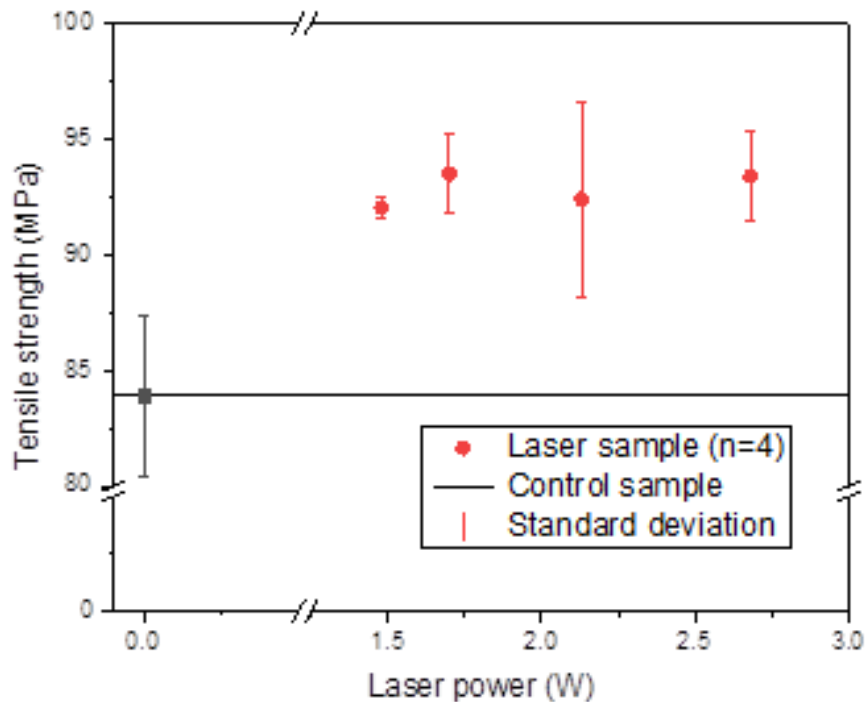


Figure 4. 4 Tensile strength of laser pre-deposition heating PEEK tensile bar and control samples.

A necking behavior was witnessed in laser samples during tensile test. Besides, fracture between layers was observed in control samples as shown in Fig. 4.6 (a). An area correction factor of 0.963 was used due to the uneven feature on the side, as shown in Fig. 4.6, while the origin of this is from the nature of fused extrusion-based process.

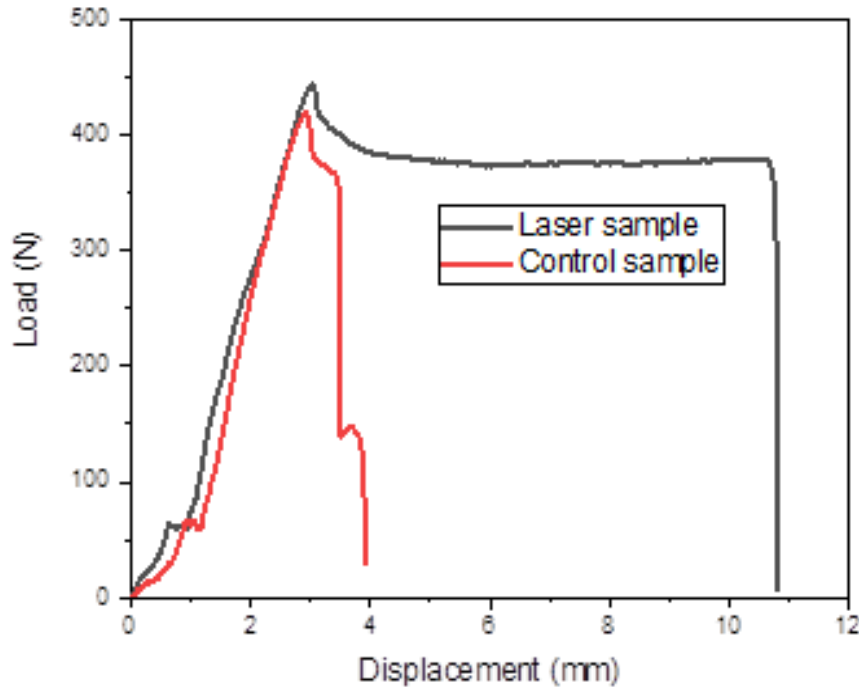


Figure 4. 5 Load-displacement curve for 1.7 W laser pre-deposition heating and control samples.

Note that tensile strength of laser pre-disposition heating sample, control sample, and material are 93.5 MPa at 1.7W, 83.9 MPa, and 100 MPa (given in Tab. 2) respectively. More specifically, tensile strength of printed part only reached 83.9% compared to that of raw material. With the laser pre-deposition heating process, tensile strength was increased by 11.4% and reached to 93.5% compared to that of raw material. The drop in tensile strength has been well elaborated in rheological model [41], in that when the material was flowing inside extruder, shear force from the friction between material and extruder wall brought stretch and disentanglement into the microstructure of polymer chains. Therefore, residual stress and unstable structure (stretch and disentanglement) could remain in printed

part if the cooling process is not slow enough to allow polymer chains to spring back or reptate [43].

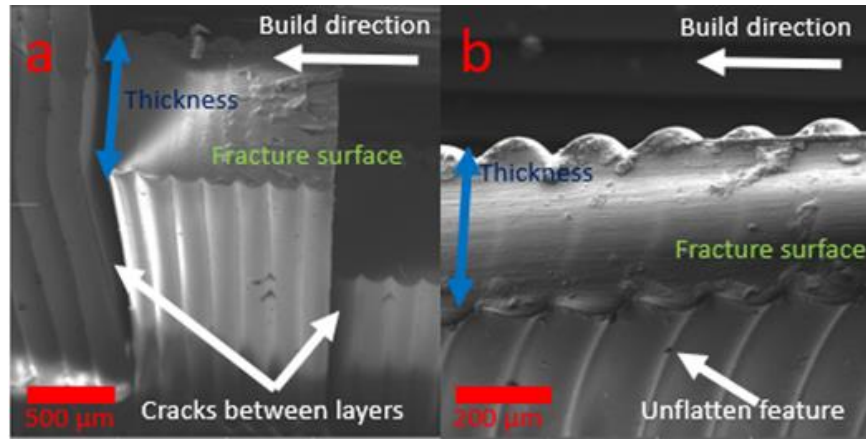


Figure 4. 6 SEM of tensile test fracture surface for (a) Control sample; (b) 2.13 W laser sample.

In this work, laser pre-deposition heating process was used to achieve a slower cooling process that would not only enhance inter-layer bonding strength [52], but also allow intra-layer microstructure to relax and therefore to reduce residual stress. The temperature profile, shown in Fig. 4.7, presents evidence of significantly slower cooling process with laser in-process heating. As has been observed from experiment shown in Fig. 4.4, the process raised the tensile strength by 9.6 MPa (11.4%) at 1.7 W of laser power. It is hypothesized that the 9.6 MPa decrease is from the residual stress generated during nozzle flow and 90° turn that described in the rheological model [41], and the process of laser heating allows relaxation of residual stress, hence appeared as an increase in tensile strength. In this hypothesis, we assumed that during the heating process when the temperature is above glass transition temperature, stretched and disentangled polymer chains were allowed to relax (spring back) as described in Fig. 4.8, and reptate[52], then result in a more entangled polymer cluster microstructure, therefore, higher tensile strength.



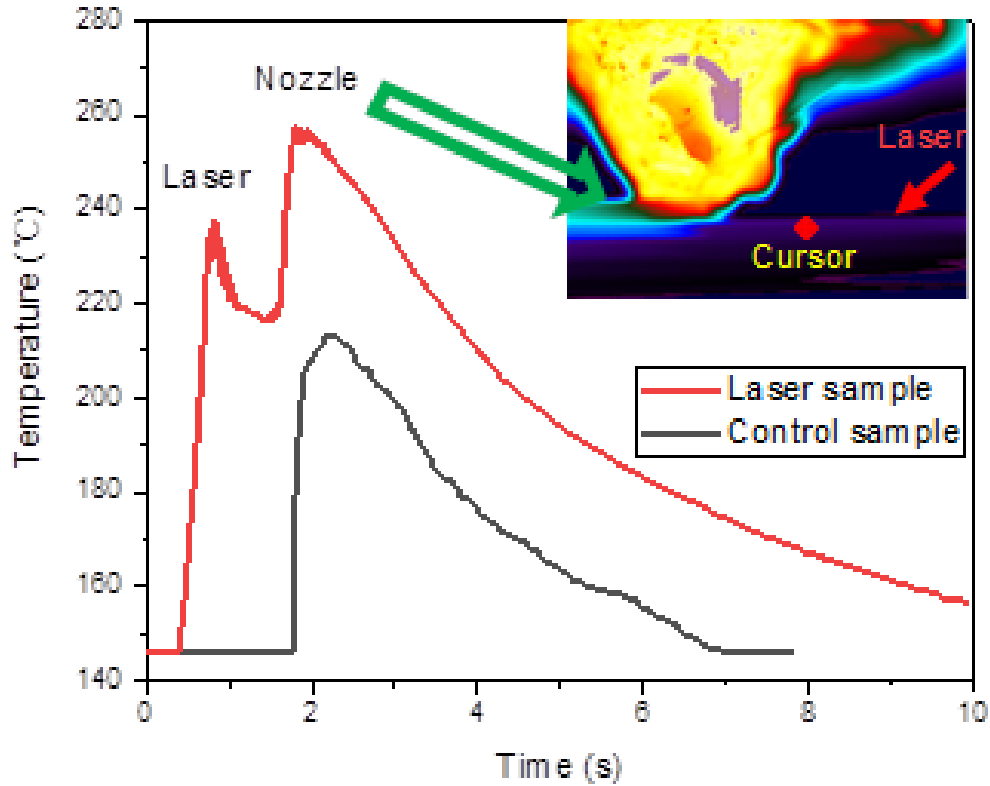


Figure 4.7 Temperature profile of sample during print. (Cursor is the point where temperature was measured).

Tensile strength of all laser samples stayed nearly around similar value. It is assumed that the maximum level of relaxation has occurred, so the laser power does not affect the strength any further. From our previous work on effect of laser on tensile strength along build direction [52], an increase in tensile strength was found until 2.13 W, then followed by a descending trend which was attributed to polymer degradation. In this work, laser power range used was from 1.5 W to 2.7 W while no trend of increase or decrease was observed, i.e. relaxation has fully happened at 1.5 W, while reptation requires a slower cooling rate (2.13 W). Besides, no decrease in tensile strength was observed at 2.7 W, proving the amount of degradation occurred is ignorable. Therefore, we assumed that relaxation occurred faster than reptation due to the driven force-residual stress, and

degradation remains only in a small thickness of the inter-layer interface that will not affect the intra-layer microstructure.

Another evidence for this hypothesis is the behavior of load-displacement curve shown in Fig. 4.5. Upon reaching the ultimate tensile strength at around 3mm displacement, the 1.7 W laser sample start to elongate at nearly constant force and finally fracture at 10.7 mm, while the control sample fractured below 4 mm displacement. The laser sample behaved quite similar to common polymer manufactured with traditional method (e.g. blow molding or injection molding), while the control sample behaved like brittle plastic. It is believed that the laser process is the factor to generate the difference in microstructure between laser and control samples, therefore result in a different fracture behavior. In the hypothesis, the reason for the difference in microstructure is that the laser sample is less stretched and disentangled, which is believed to be similar to Fig. 4.8 (b), while the control sample is more stretched and disentangled as described in Fig. 4.8 (a). In this situation, if a force is applied to the two sides of a sample, the polymer chains should initially get stretched, elongated and then break when it reaches the maximum point. Because the polymer chains in control sample are more stretched and disentangled, less elongation is allowed before pulling polymer chains out or breaking polymer chains. While in laser sample, more elongation is allowed due to the existence of more recoiled and entangled polymer chains, therefore the polymer chains were initially got stretched and then broke. As a result, the

elongation for control and laser sample are 3.5 mm and 10.7 mm, respectively; hence the load-displacement curve supports the hypothesis.



Figure 4. 8. Schematic diagram of Reptation and Relaxation(a) Initial state: stretched and disentangled; (b) After relaxation: cluster shape, entangled

Moreover, during the elongation, necking behavior was observed in laser sample. As shown in Fig. 4.6, thickness of fractured laser sample is significantly smaller than that of control sample. The necking behavior happened along the width direction as well. Note that the pre-deposition laser heating process enhanced reptation between layers therefore the interlayer strength is almost as strong as the control sample which was proved in our previous work [52]. Thus, fracture between layers along build direction was only observed in control sample. It is confident to say that the laser pre-deposition process significantly improved the tensile behavior.

#### 4.4 CONCLUSIONS

In this work, the effect of laser pre-deposition heating process on tensile strength and tensile fracture behavior of FFF-printed PEEK along in-plane direction was presented. Tensile strength of laser pre-deposition heated sample at 1.7 W reached 93.5 MPa, which increased by 11.4% compared to control sample. Laser sample also result in significantly larger elongation before fracture. Besides, necking behavior was observed in laser sample. It is believed that laser enhanced relaxation to happen at intra-layer, therefore increased

tensile strength and elongation before fracture. The relaxation appeared to be fully occurred in all laser samples regardless of laser power level. Based on these results, laser pre-deposition heating is considered as a viable means of improving mechanical behavior of parts from extrusion-based 3D printing processes.

## CHAPTER 5

### INTERFACE HEALING BETWEEN ADJACENT TRACKS IN FUSED FILAMENT FABRICATION USING IN-PROCESS LASER HEATING

#### 5.1 INTRODUCTION

Additive manufacturing (AM), also known as 3D printing, is layer by layer fabrication process of a 3D object from computer aided design (CAD) model or a digital 3D model [53,54]. Fused filament fabrication (FFF) has become a preferred additive manufacturing method for thermal plastic materials due to its cost effectiveness and feasibility [1,55,56]. While an expensive mold is required before fabrication for most traditional methods to fabricate thermoplastic parts, such as injection molding and blow molding. In FFF process, two rollers are used to push the filament of thermoplastic material through a heated nozzle that is above the glass transition temperature of the filament, then the softened filament was deposited and bonded in a track-shape on build plate or previously deposited material layer [2,57]. To control the deposition process, a slicing software is used to slice and reproduce the 3D model into G-code command that controls movement of nozzle and build plate, extrusion speed, temperature, and other process parameter for a 3D printer to execute [3]. Although, FFF has numerous advantages, including the diversity of printable material [4–6,47,48], capability of multi-material composition printing [58], ability of fabricating tiny or huge object [1], and even biomedical parts [59,60]. Parts fabricated using this method are anisotropic [45].

The anisotropic property of FFF built object is due to the mechanism of the extrusion-based process. In this process, filament was extruded from a nozzle with diameter change usually from 1.75 mm to 0.4 mm and deposited flatly on build plate with models built as “nozzle

flow” and “90 ° turn” [41,43,50,52]. As explained by these two models, polymer chains are highly stretched and disentangled in deposited tracks, especially at the region near the track surface [43,61]. In order to make the printed part isotropic, fully reptation and relaxation are required for the polymer chains at the surface of the deposited track and at the interface between tracks. Both relaxation and reptation are time and temperature dependent functions[43,52,61], that polymer chains are capable of fully relaxing and entangling to form solid microstructure similar to parts fabricated using traditional method, if enough time at high temperature is permitted. However, during the deposition process, extruded filament was deposited on or next to a previously deposited tracks that were at a lower temperature, which does not allow reptation and relaxation to fully occur [45,52]. Therefore, the mechanical strength of parts fabricated with FFF is anisotropic with the weak region located at the interface between deposited tracks.

A number of works were aimed on improving the mechanical strength of FFF build objects. There are many works on improving the interlayer bonding strength by optimizing printing parameters, such as nozzle temperature [62–65], build plate temperature [66,67], print speed [65,68], layer thickness [69–72], and raster strategy [20,22]. However, the effectiveness of optimizing printing parameter is restricted due to the mechanism of FFF. Post-process work has also been done by annealing the printed part to increase bonding strength with significant improvement in bonding [73,74]. In-process approaches using laser heating [45,52,61] and ultrasonic vibrating [44] has also achieved considerable result on healing inter-layer interface. However, all of the work were focusing either on the bonding strength at inter-layer interface (which is the weakest direction in FFF built part) or mechanical strength along in-plane direction. None of these works were focusing on the

healing process between adjacent tracks in the same layer because the direction of the deposited track can be easily altered to make the mechanical strength consistent along all in-plane direction. Even if the interface between adjacent tracks is not healed.

In this work, the effect of in-process laser assisted method on healing the interface between adjacent tracks in the same layer was investigated. An in-process laser pre-heating apparatus was designed and implemented. The interface between adjacent tracks of control and laser assisted samples were thoroughly characterized and compared. The mechanical strength of samples with different laser samples were tested, as well as the flexural behavior.

## 5.2 METHODOLOGY

### 5.2.1 LASER PRE-HEATING APPARATUS

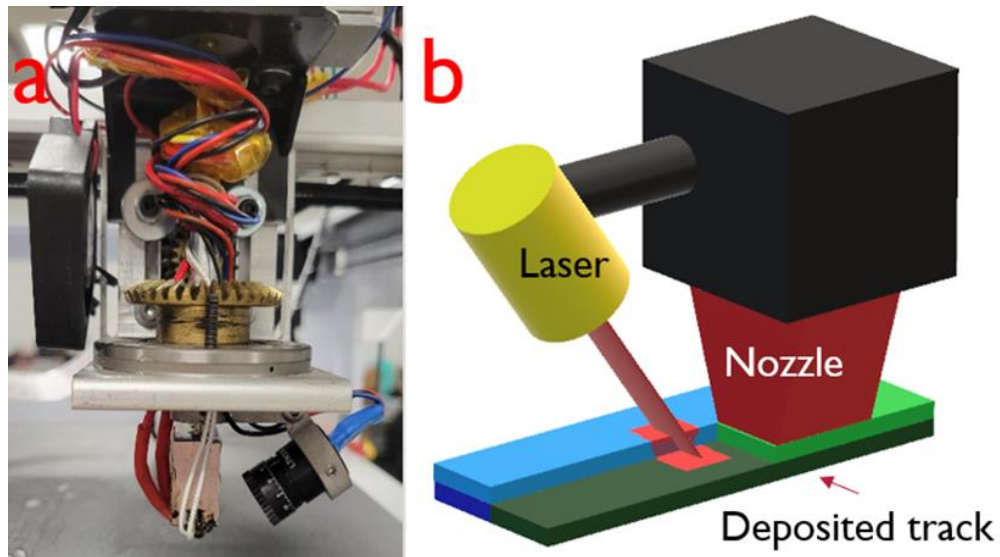


Figure 5.1 (a) photo of the laser pre-heating apparatus, (b) schematic diagram of the process

A commercial 3D printer (Type A Machine Series 1, San Francisco, US) was used as the platform for the laser pre-heating apparatus. The motherboard of the printer was replaced with a Duet 2 Wifi (Duet3D, UK) for rotation control. Shown in figure 1 a is a photograph

of the laser (808 nm) pre-heating apparatus implemented. In order to rotate the laser along x-y plane. A stepper motor-controlled by rotation command from the mother-board-was mounted behind the gear to allow rotation of the bottom part which include the laser diode and the hot end. Therefore, the position of the focused laser spot could be controlled using G-code even during print. To generate the G-code for this apparatus, a customized G-code convertor was programmed to add rotation command when the moving direction of the nozzle changes. Hence, the laser spot was always focused on the boundary of the pre-deposited adjacent track and the track that will be deposited. More specifically, half of the intensity falls on the adjacent layer (current layer, marked in light blue), while the other half falls on the previous layer (one layer lower than the current layer, marked in dark green) as shown in figure 1 b. The shape of laser spot is rectangular with a length of 1 mm and a width of 0.5 mm.

### 5.2.2 SAMPLE PREPARATION

Black PLA filament (MakerGear, Beachwood, US) was used as the material. The print parameters are shown in table 1. The raw sample printed was a Multi wall rectangular bulk as shown in figure 2 a. The dimensions of the raw sample 80 mm by 50 mm by 5 mm. Then the raw sample was cut into 4 mm wide bars (along the red dash lines shown in figure 3 a) using a diamond cutter (Preciso-CL, Top Tech Machines Co. LTD, Taichung, Taiwan) for bending test. Same process was repeated for samples with laser powers from 0 to 250 mW.

Table 5.1 Print parameters

Parameter	Data
Nozzle diameter	0.8 mm



Extrusion width	1 mm
Layer height	0.2 mm
Extrusion Temperature	195 °C
Bed temperature	60 °C
Print speed	10 mm/s

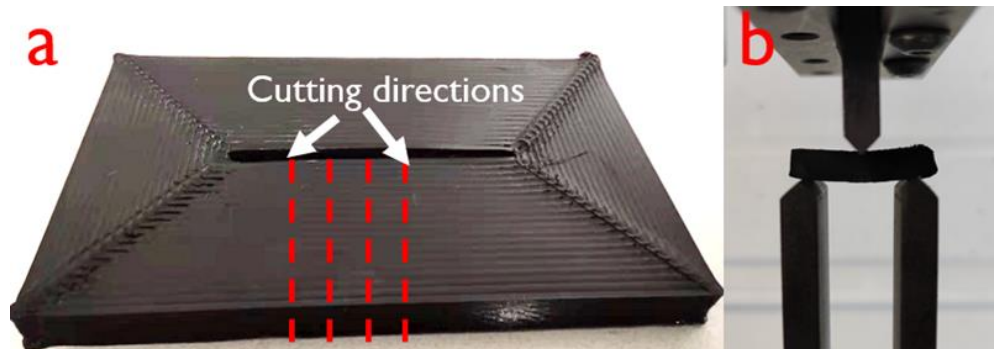


Figure 5.2 (a) Printed sample and cutting direction of flexural bar. (b) 3-point flexural test

### 5.2.3 MECHANICAL TEST

An MTI-2K tensile testing machine (Measurement Technology Inc. Marietta, US) and a set of customized 3 point bending stage was used for flexural test. In each laser power group, data of 4 samples were collected. The pre-load for flexural test was set to be 30 N and the pushing rate was 5 mm/min. Thickness of all flexural sample are 5mm [75]. Due to the possible error from diamond cutter, width of every single sample is measured before each test and was used for calculation of flexural strength. The distance between the two lower points for 3-point flexural test is 15.11 mm (measured). The flexural test is shown in figure 2 b. Due to the thickness of the flexural bar, the bottom of the bar suffers from tensile while the top of the bar suffers from compression.

### 5.2.4 TEMPERATURE PROFILE

Thermal profile of the top surface was measured using a FLIR a6753sc thermal camera (FLIR, Wilsonville, US). The highest temperature measured at the laser spot was considered as the temperature of the pre-heating spot. The Temperature vs. laser power

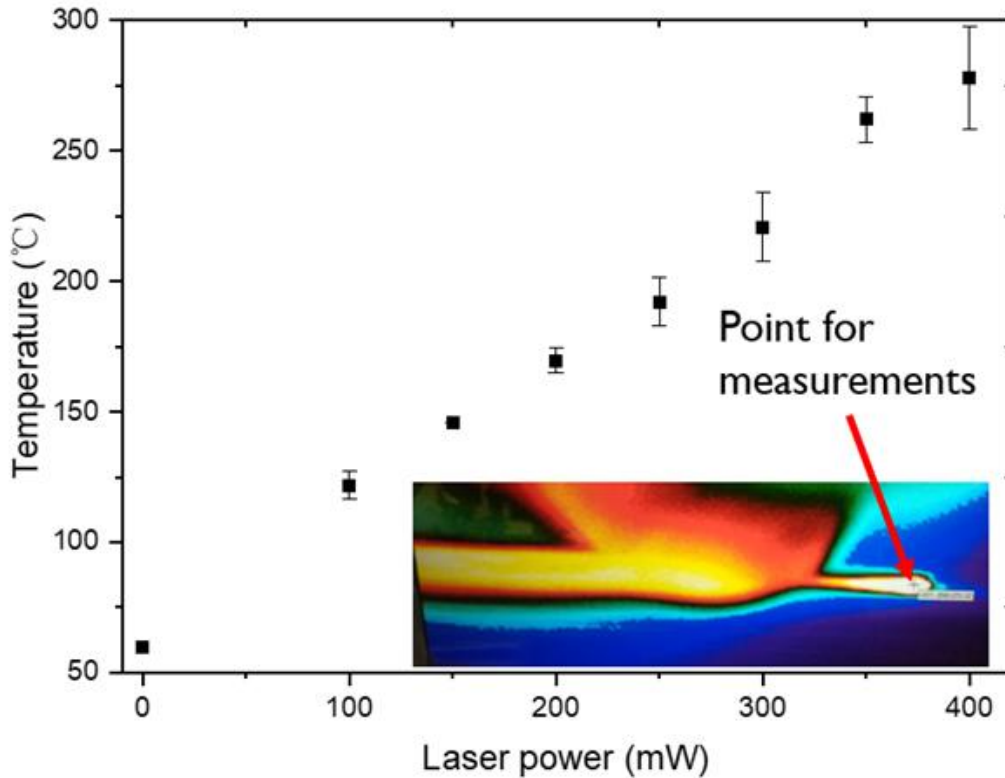


Figure 5.3 Thermal profile of laser pre-heated spot

plot is shown in Figure 3. Due to the mechanism of fused filament fabrication and size of thermal camera, the thermal measurement was performed from the side with a  $37^\circ$  angle above build plate. Therefore, the temperature profile is used only as a reference but not for calculation. A thermal image taken during print is shown in Figure 3.

### 5.3 RESULTS AND DISCUSSION

Shown in figure 4 is the flexural strength of laser assisted sample and references. The lower horizontal line represents control sample without laser pre-deposition heating. The

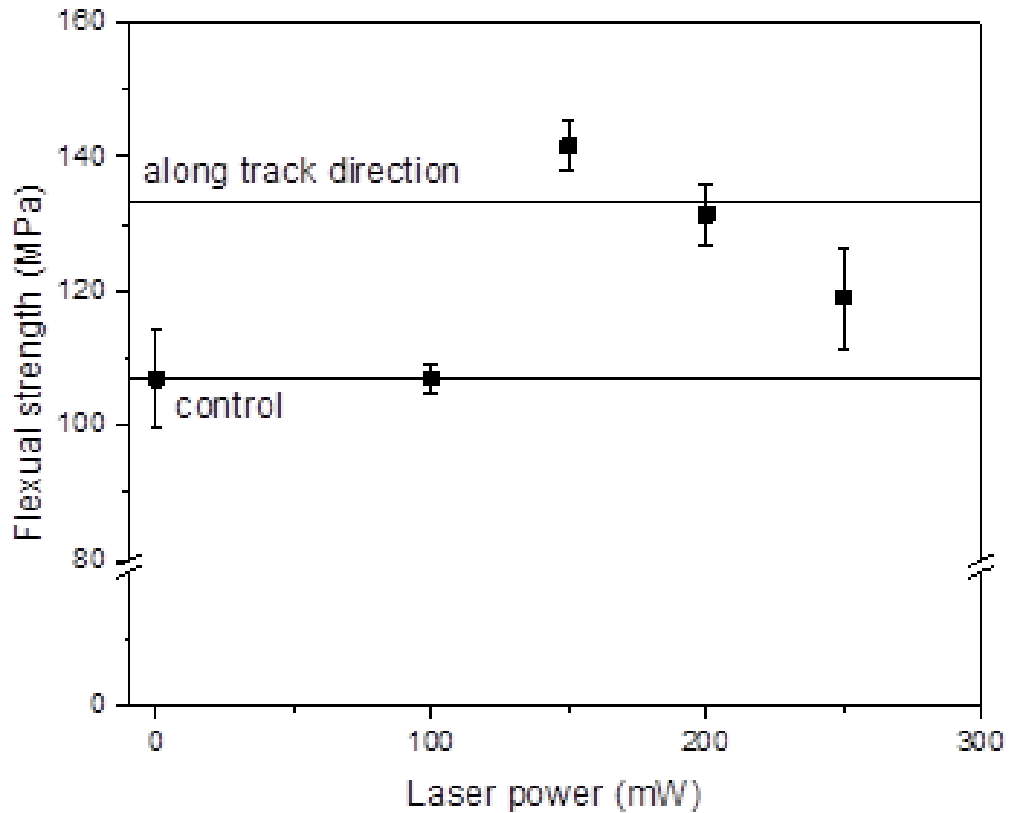


Figure 5.4 Thermal profile of laser pre-heated spot

upper horizontal line represents the strength along filament track direction by breaking the deposited tracks along the length direction instead of parallel to the interface between them. The flexural strength of control sample (based on adhesion between adjacent tracks) shows 80.3% that of samples along track direction. With the laser pre-heating process, the flexural strength of 150 mW laser sample achieved 106% compared to that of samples along track direction. The 6% increase can be explained by previous research [61], that 10% increase in mechanical strength along track direction was noted with the usage of laser, while it is still weaker than the raw material. Hence, the flexural strength of 150 mW still lies in a reasonable range. Therefore, this process has shown the effect of resolving strength anisotropy by healing the interface between adjacent deposited tracks. A decrease of the flexural strength was observed above 150 mW. This trend is expected to be the outcome

of polymer degradation, which has been seen in previous works [45,52]. No significant effect on flexural strength was witnessed with the usage of 100 mW laser pre-deposition heating. It is considered to be the consequence of temperature threshold of thermal diffusion not being reached.

The effect of laser pre-heating on flexural strength between adjacent deposited tracks can be explained using the following equation proposed by Ezekoye [34].

$$\frac{\sigma_t}{\sigma_{max}} = \left( \frac{t_{weld}}{\tau_{rep}} \right)^{1/4} = \left( \frac{t_{weld} D_s}{R_g^2} \right)^{1/4} \quad \text{Equation 5.1}$$

Where  $\sigma_t$ ,  $\sigma_{max}$  are the strength of the interface and the strength of the bulk material respectively,  $t_{weld}$  is the healing time of the interface (or time during which the interface stays above glass transition or melting temperature),  $\tau_{rep}$  is the reptation time (time needed for polymer chains to reptate as far as  $R_g$ ),  $D_s$  is the center of mass diffusivity of polymer chains (a function of temperature), and  $R_g$  is the radius of gyration of polymer chains.

Both  $D_s$  and  $\tau_{weld}$  are positive temperature dependent functions, and the mechanical strength  $\sigma_t$  is dominated by these two values. Therefore, the mechanical strength is only controlled by the temperature at the interface if the material (radius of gyration) is set. With the application of laser pre-heating process, the interface temperature increases, then it allows larger amount of mass transfer through the interface to heal the interface, and eventually increases mechanical strength by enhancing the entanglement of polymer chains at the interface.

Aside from the mechanical strength, the interface healing from laser pre-heating process also affected the displacement before fracture. Shown in figure 5 is the displacement of

sample along vertical direction (measured at the upper tool in the 3-point bending test shown in figure 2 b) before flexural failure or ultimate strength (for samples along track

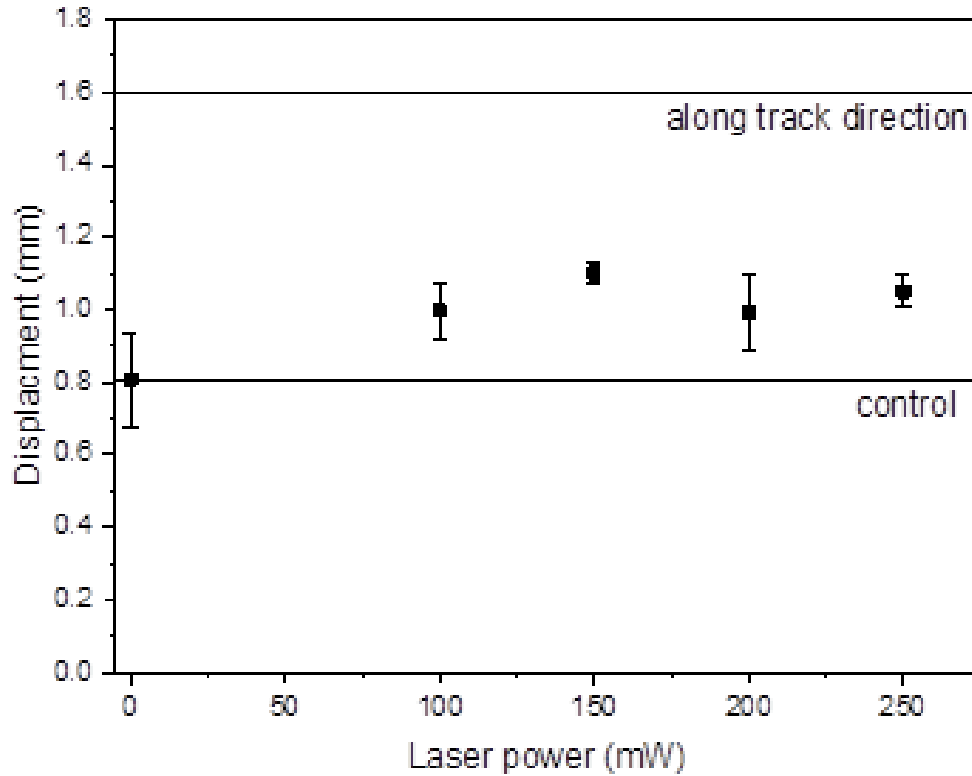


Figure 5.5 Displacement before flexural failure or ultimate strength (for samples along track direction).

direction). All laser samples show similar displacement value and are all higher than the control sample. The displacement of 150 mW laser samples shows slightly higher value than all other samples and has reached 68.8% of samples tested along track direction. While the control sample is only 50.1% compared to that of samples along track direction.

The load-displacement curves of one sample in each group for control samples, 150mW laser samples and samples along track direction are shown in figure 5. Please note that the flat region from 0 to ~ 0.6 mm is not counted as displacement. Both control sample and 150 mW laser sample show stiffer behavior than sample along track direction. The highest load and slop data for laser samples were observed at 150 mW.

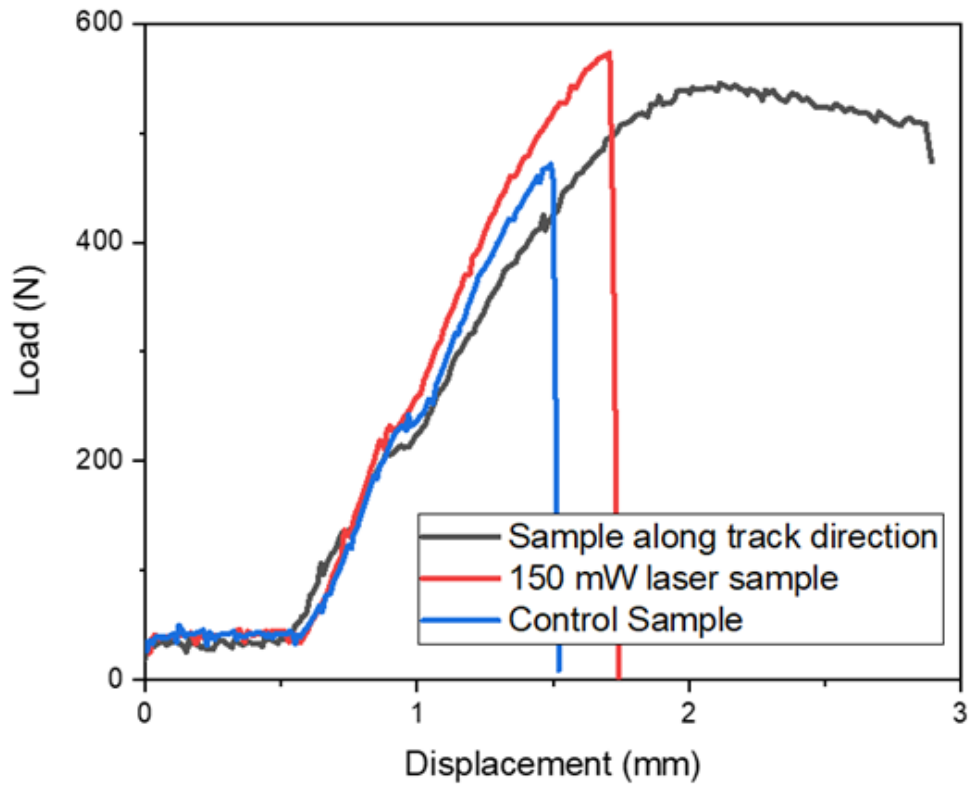


Figure 5.6 Load-displacement curve of samples in different groups

In the load-displacement curve shown in Fig 6, the curve of 150 mW laser sample is slightly stiffer than that of the control sample, and the flexural strength of the 150 mW laser sample is significantly higher. The difference is attributed by the interface healing induced by the laser pre-deposition heating process. To be more specific, with the laser pre-deposition heating process, higher interface temperature was achieved and result in longer time for mass transfer across the interface (reptation) and relaxation. Relaxation is, when stress in a linear polymer relaxes through a curvilinear diffusion and finally confined into a tube region for reptation [61]. Hence, the fracture mechanism of control sample contains a higher percentage of pulling disentangled polymer chains out, while that of the 150 mW laser sample contains a higher percentage of breaking entangled polymer chains. In the sample along track direction that no laser heating process is involved, a higher percentage

of polymer chains are orientated along the same direction with a lower amount of entanglement due to the nozzle flow and 90 ° turn. The fracture mechanism becomes

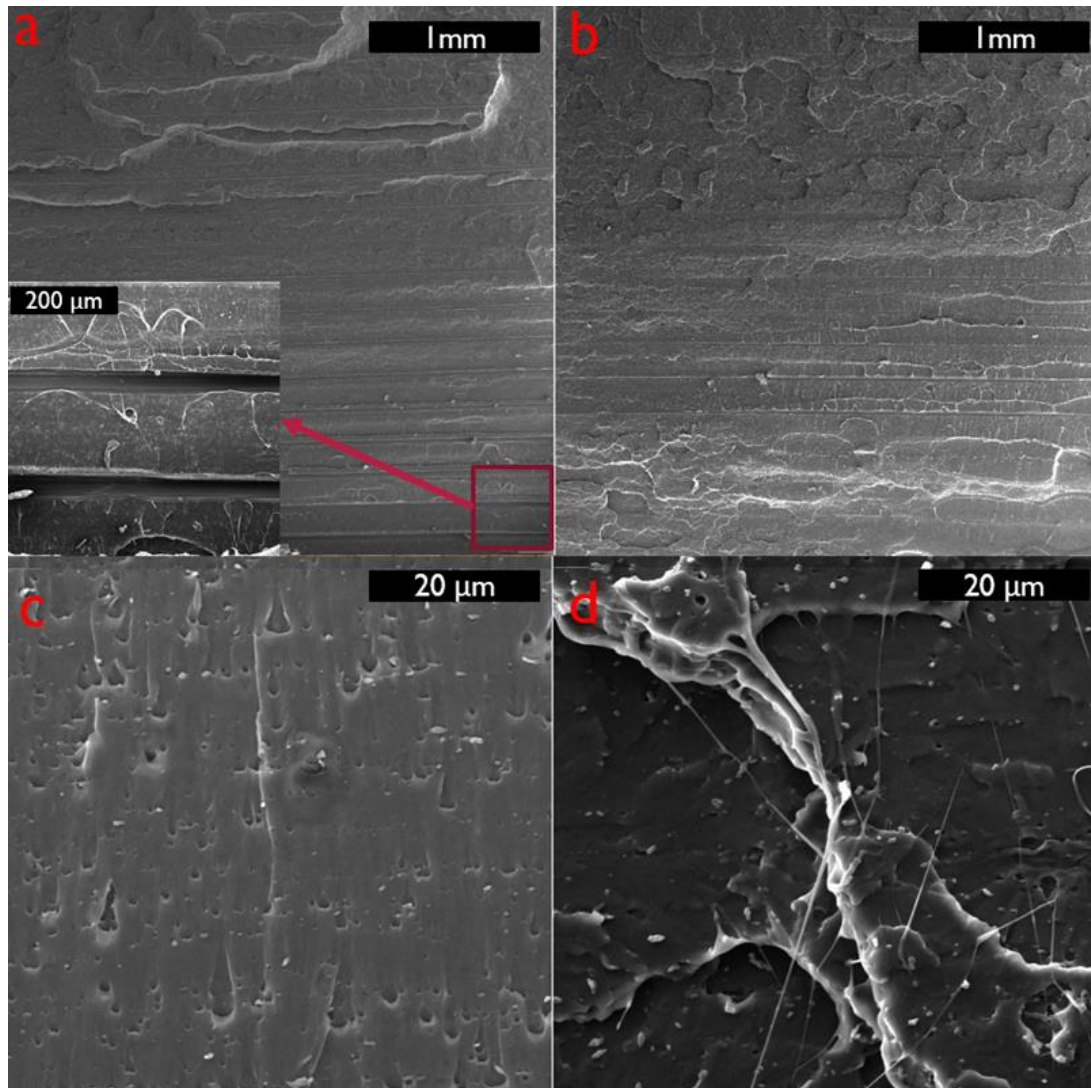


Figure 5.7 SEM image of flexural surface at different scales. (a) (c) Control sample, (b) (d) 150 mW laser assisted sample

elongating and breaking/pulling out polymer chains. Besides, necking behavior has been observed for lower layer during flexural test. Therefore, the lower flexural strength of sample along track direction can be explained by lesser amount of entanglement and reduction of width during test.

The micro image of the fracture surface (between adjacent tracks) taken using SEM is shown in figure 7. Shown in figure 7 a and b are the overall view of control and 150 mW laser sample, respectively. The bottom shown in the figures represent the bottom of sample during flexural test in figure 2 b. In the flexural test, the bottom of the sample faces tension while the top of the sample faces compression. Thus, the SEM image focused only on the layers at the bottom since it is the location where fracture started. The photo at bottom left that enlarged the local region in figure 7 a clearly shows the interface of adjacent tracks in three layers. Gaps are observed between tracks from neighbor layers. Clearly, in the 150 mW laser sample shown in figure 7 b, no gap between tracks at the same region was witnessed. At higher magnification shown in figure 7 c and d, the control sample (c) appears to have a smoother fracture surface, while that of 150 mW laser sample (d) seems to be rougher with string-shape surface feature.

The gaps between tracks shown in figure 7 a represent the weakest region in FFF 3D printed parts. It is a line shape region located at the intersection of two planes: inter-layer interface and the interface between adjacent tracks. The fracture started at this region when tension is applied. The laser pre-heating process heated directly on the weakest region (edge of track), therefore enhanced mass transfer of polymer chains in the region and reduced the anisotropic behavior. Furthermore, the fracture surface of the tracks in control sample exhibit less plastic deformation. In comparison, that of 150 mW laser sample shows significant string-shape material pulling-out feature. This result further verified the reptation across the interface between adjacent tracks.



#### 5.4 CONCLUSIONS

The effect of laser pre-heating on interface healing between adjacent tracks of PLA using fused filament fabrication was investigated. Flexural test was performed on control and laser pre-heating bending samples. The effects of laser pre-heating on flexural behavior and energy microstructure interaction were observed and discussed. An increase of flexural strength between adjacent tracks to up to 106% of that along track direction was found, as well as an increase in displacement before fracture from 50.1% to 68.8%. The effect associated with the use of laser pre-heating are attributed to the thermal-induced increase in polymer reptation and relaxation, therefore resulting in entanglement at the interface between adjacent tracks.

## CHAPTER 6

### IN-PROCESS ROTATING LASER-ASSISTED SURFACE HEALING IN FUSED FILAMENT FABRICATION

#### 6.1 INTRODUCTION

Additive manufacturing (AM), known as three-dimensional (3D) printing, is a fabrication process to build 3D objects layer by layer based on computer aided design (CAD) model or digital 3D model [53,54]. Fused filament fabrication, an additive manufacturing method, is one of the most desired process for 3D printing of thermal plastic materials due to its capability and cost-effectiveness [1,55,56]. In comparison to the traditional methods such as injection molding and blow molding, FFF does not require expensive molds to build complex objects. The process of the FFF starts from thermal plastic filament being pushed through a heated nozzle that stays above the glass transition temperature of the material by two rollers, then 3 motors for X Y and Z axis are used to control the position of deposition. With the movement of the deposition position, a 3D object can be built up layer by layer [2,57,76]. In order to control the movement of the three axis, the extrusion, and the temperature setting, a slicing software is used to slice the 3D model in to layers and to compile it into G-code that can be read by the 3D printer for different materials, time lengths, and print qualities [3]. Even though FFF has enormous benefits, such as diversified application field including biomedical [59,60], aerospace [1,77], microfluidic and sensor in electric area [78–80], as well as the variety of printable material [4–7,18,44]. The surface finish of FFF printed part exhibit is limited by the layer-by-layer fabrication process itself.

The limit on the surface finish is from the mechanism of the extrusion-based process. Fused filament fabrication process builds 3D object layer by layer, while the thickness of the layer is usually 0.1 or 0.2 mm [61], therefore results in a boundary between layers. Moreover, the cross-section shape of the extruded material is round, which result in a curved surface at the edge of the deposited track. Hence, the side surface of FFF 3D printed object has a wave-shape feature as the top two layers shown in figure 1 b.

A large number of works has been done to improve the surface finish of FFF printed objects. Many of them were focusing on optimizing print parameter to improve the geometrical accuracy and the surface finish [81–87]. Some works were done on simulations to predict the surface roughness from print parameter [18,88–91]. To further improve the surface roughness, post-process techniques were used, such as hot cutter to improve surface finish [88] and CNC milling machine [92], these two applications achieved decent surface finish but are limited by the size of the sample. Chemical post-process treatment was also investigated [93–95]. Laser post-process treatment was firstly used on metal for surface finish [96–99], then it stated to be used to improve surface for FFF printed object [100–102]. However, all these solutions either failed to fully solve the problem or requires a post-process method, that significantly increases the expense of the process.

## 6.2 METHODOLOGY

### 6.2.1 ROTATING LASER SURFACE HEALING APPARATUS

The rotating laser surface healing apparatus was built on a Type A machine 3D printer (Type A Machine Series 1, San Francisco, US). In order to add a rotation axis control, a Duet 2 Wifi (Duet3D, UK) was used as a replacement of the motherboard. The implementation of the rotating laser head is shown in Fig 1 a, the filament is feed from the top and pushed by two rollers in a long Teflon tube into the hot end at the bottom. A customized L-shape aluminum bracket was used to hold the horizontal gear for rotating laser control with the hot end and a vertical gear with the driven stepper motor. Wires for heater, thermistor and laser power were coiled on the Teflon tube. The laser (808 nm) was installed on the hot end with a customized adjustable elbow-shape holder. Therefore, the hot end and laser setup rotate together. Due to the restriction of the wire, the permitted rotation is from 0 to 360 °.

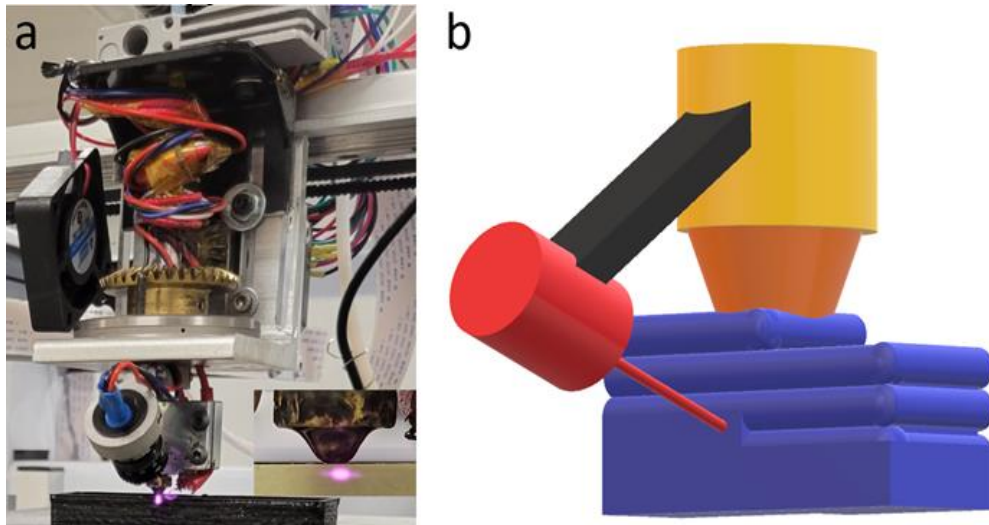


Figure 6.1 (a) rotating laser healing apparatus, (b) schematic diagram of the healing process

In order to create the G-code with rotation command. The 3D part file was firstly sliced and output into an original G-code file using Simplify3D, then to control the position of the laser focused point. A customized software was made using LabVIEW to add rotation command into the G-code to guarantee that the position of the laser point is on the side, as shown in Fig 1 b. Therefore, the laser will rotate to the correct position before the alternation of the nozzle moving direction. The laser focal point is in rectangular shape (1 mm by 0.6 mm), and it is focused at 0.6 mm below the nozzle as shown in Fig 1 a. The surface healing works in-process and does not require any post-process thermal treatment.

#### 6.2.2 THERMAL PROFILE

The thermal profile of the laser heated region during printing was measured using a FLIR a6753sc thermal camera (FLIR, Wilsonville, US) that placed horizontally in front of the healed surface. The size of the melting pool region varies with laser power and printing speed. The highest temperature in the melting pool was used as a reference for the thermal profile. Shown in Figure 2 is the temperature vs. laser power plot. The thermal image in Figure 2 is taken at 5 mm/s print speed and 700 mW laser power.

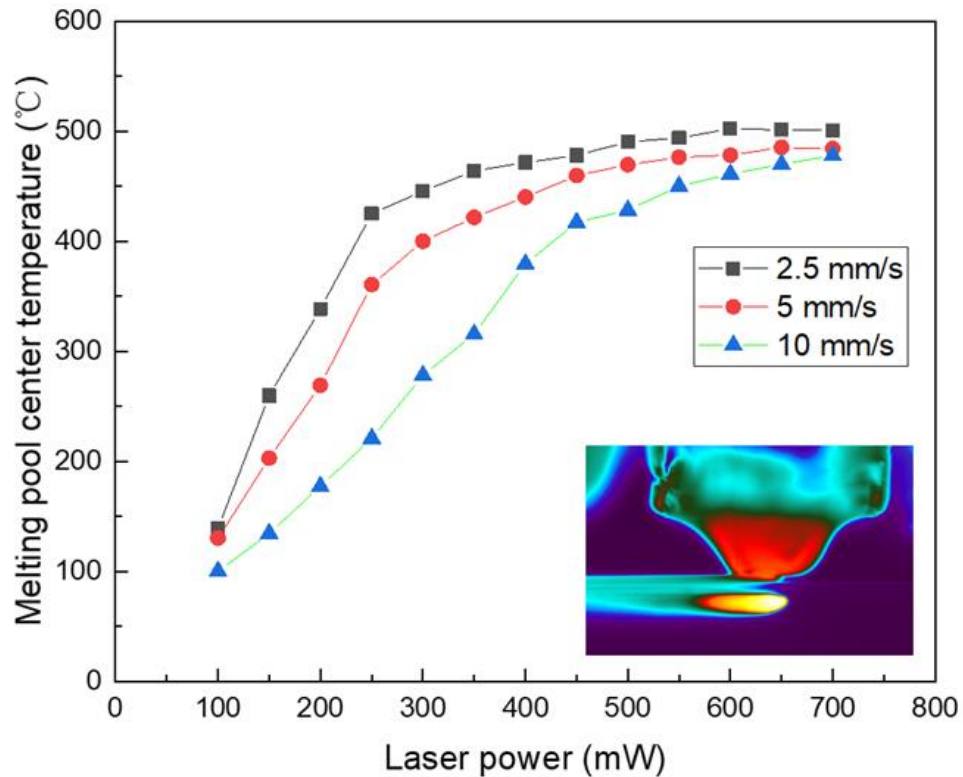


Figure 6.2 Temperature profile of melting pool at different laser power and printing speed

### 6.2.3 SAMPLE PREPARATION

All prints were fabricated using the rotating laser surface healing apparatus introduced above. The filament used for the prints is black PLA (MakerGear, Beachwood, US). A 0.8 mm E3D brass nozzle was used for all prints. Deposited track width is set to be 1 mm wide and 0.2 mm thick. 195 °C nozzle temperature and 60 °C build plate temperature were maintained. Three print speed (2.5 mm/s, 5mm/s, 10 mm/s) and thirteen laser power (100 mW to 700 mW, with a 50 mW interval) settings were investigated. The output laser power was measured using a power meter (Thorlabs, Newton, US).

Three groups of samples were prepared.

1. Surface roughness sample. In this group, three samples for the three print speeds were fabricated. Each sample is a single wall rectangular box without top and bottom. The size of the box is 80 mm long, 20 mm wide, and 40 mm tall. Since the layer height is 0.2 mm, the box is sliced into 200 layers by the slicing software. 10 layers (2 mm height) was used for each laser setting. The rest 14 mm height was left at top (8 mm) and bottom (6 mm), printed as control layers without laser. Error data that from the extrusion stepper motor such as significantly narrower deposited track, was removed.

2. Tensile test samples were printed at 5 mm/s from 0 mW (control) to 700 mW laser power with a 100 mW interval. The originally printed part was a single wall rectangular box without top and bottom as shown in Figure 3 a. A desktop PCB milling machine (Bantam tools, Peekskill, US) was used to mill 5 sample out from the front wall shown in Fig 3 a with water cooling to avoid melting. The size of the tensile bar [45,52] is shown on Fig 3 b. Standard tensile bar design was not used, because the focus of this work is only on the exterior surface. More errors will be induced if longer and thicker tensile bar was used.



Figure 6.3 (a) Printed rectangular box without top and bottom for tensile test (b) milled tensile bars

3. Curved surface healing sample. A customized hose adaptor was designed and printed to demonstrate the capability of the surface healing process on curved surface. The diameter of the bottom and top are 20 mm and 12 mm, respectively. The height is 34 mm.

#### 6.2.4 SURFACE ROUGHNESS

A Dektak 8M profilometer (Veeco, Plainview, US) was used to characterize the surface of printed samples. The force applied was 3 mg. Scan length was 34 mm and the duration was 80 s. The resolution of acquired data was 1.417  $\mu\text{m}$ .

#### 6.2.5 MECHANICAL TEST

An MTI-2K tensile testing machine (Measurement Technology Inc. Marietta, US) was used to perform the test for the milled tensile bars. In each group, 4 samples out of the 5 were tested and the 1 left was used as a replacement of abnormal data or failed test. The pre-load for the tensile test was set to be 30 N and the pulling rate was set to be 5 mm/min.

### 6.3 RESULTS AND DISCUSSION

#### 6.3.1 SURFACE ROUGHNESS

Shown in Figure 4 is a comparison of surface morphology between control sample and 2.5 mm/s at 700 mW laser treated sample, with optical image on the right side. A remarkable surface healing performance was observed that the surface turned from wave-shape with a rough 58  $\mu\text{m}$  wave height to nearly flat surface.

The plot of profile roughness parameter ( $R_a$ ) at 3 print speed and 14 laser powers (0 mW for control sample) were shown in Figure 5. The roughness parameter for the control sample is at around 15  $\mu\text{m}$  for all 3 print speeds.



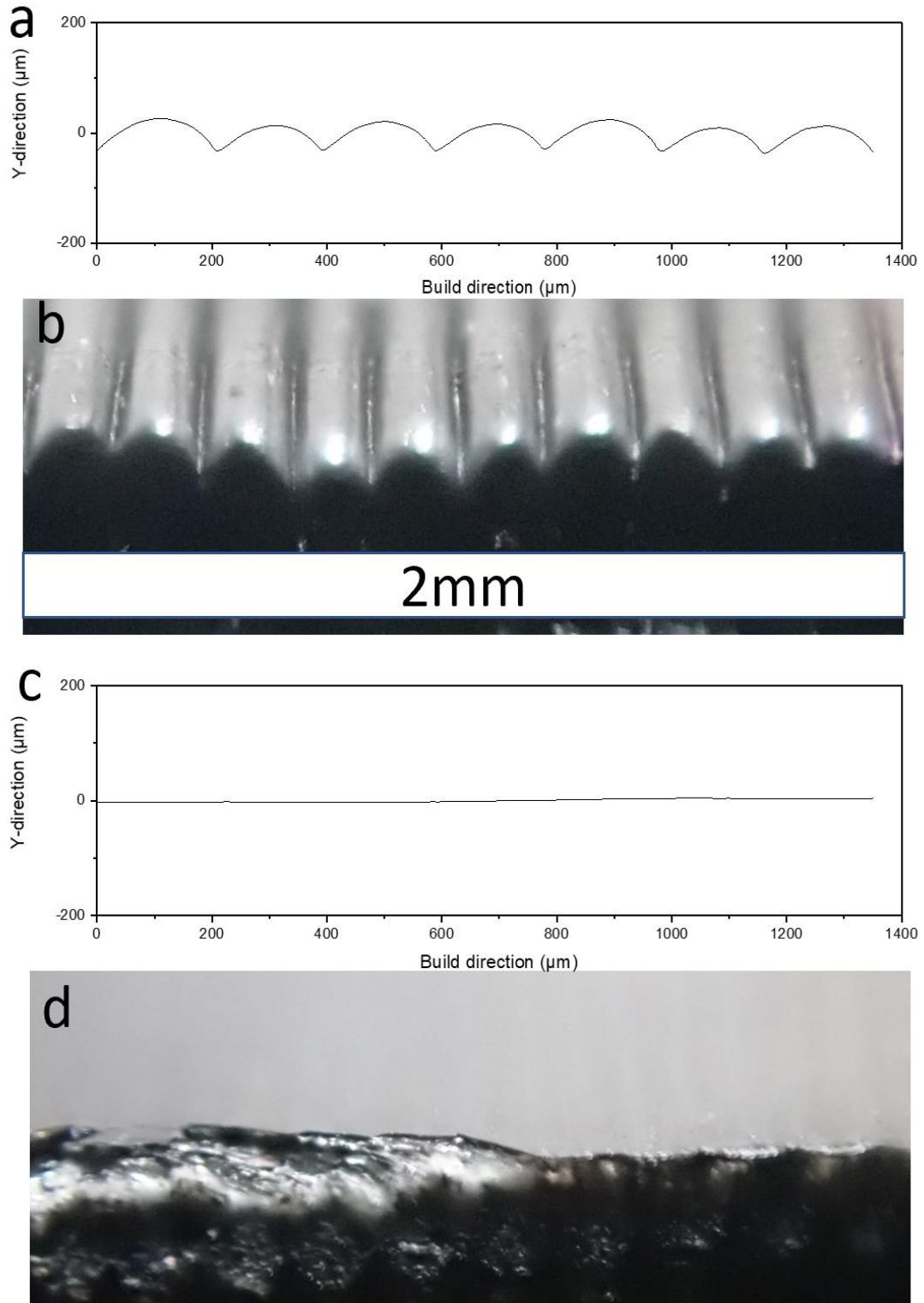


Figure 6.4 profilometry data of control (a) and 2.5 mm/s 700 mW laser (c) sample, Optical image of control (b) and 2.5 mm/s 700 mW laser (d) sample from the side (same scale bar).

As shown in Fig 5 in blue triangle, the Ra of the 10 mm/s group was not significantly

affected by laser up to 450 mW. It was also observed that the visible surface healing start at 450 mW as shown in Fig 6 b, then the healing feature on the surface improved with the increase of laser power up to 700 mW. Compared to the control sample, samples in the 10 mm/s group exhibit slightly better surface smoothness, but light reflection behavior enhanced significantly (like a polishing effect). Therefore, due to high print speed, the power density of laser is not strong enough to fully heal the gap and curvature of the feature shown in Fig 4 a, but it polished the side of the deposited track. Still, laser power below 400 mW at 10 mm/s are not showing clearly reflection improvement. As shown in figure 2, at 10 mm/s, the temperature of melting pool increases with laser power almost linearly up to 400 mW at 380°C, then it turned to be steadier after 450 mW at 417 °C with a lower slope. Therefore, it is considered that around 417 °C at center of the melting pool is necessary to allow significant healing at the surface at 10 mm/s.

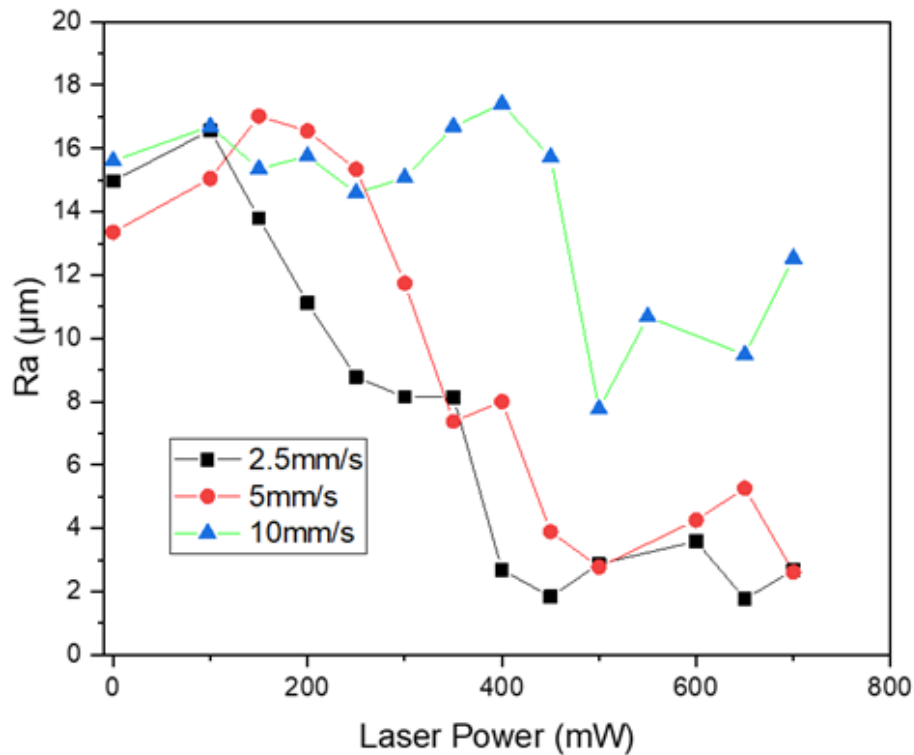


Figure 6.5 Surface roughness plot

The Red line with red circle shown in Fig 5 represents the Ra of 5mm/s laser healed group. The Ra stays steady from 0 mW laser power (control sample) to 250 mW. Visible difference in Reflection was observed at 300 mW (which represents 400 °C from figure 2), while that matches where the Ra starts to decrease with the increase of laser power in Fig 4. Remarkable improvement in surface roughness was achieved above 450 mW, with a melting pool temperature of 460 °C. Note that the time length that the melting pool stays at higher temperature is longer due to the slower print speed when compared to the result at 10 mm/s. Therefore, even though the melting pool temperature of 600 mW at 10 mm/s is 461 °C, the Ra is still substantially higher. Moreover, the actual input laser power on the surface is laser power divided by print speed, which means the actual laser power of 600 mW at 10 mm/s and 300 mW at 5 mm/s are the same.

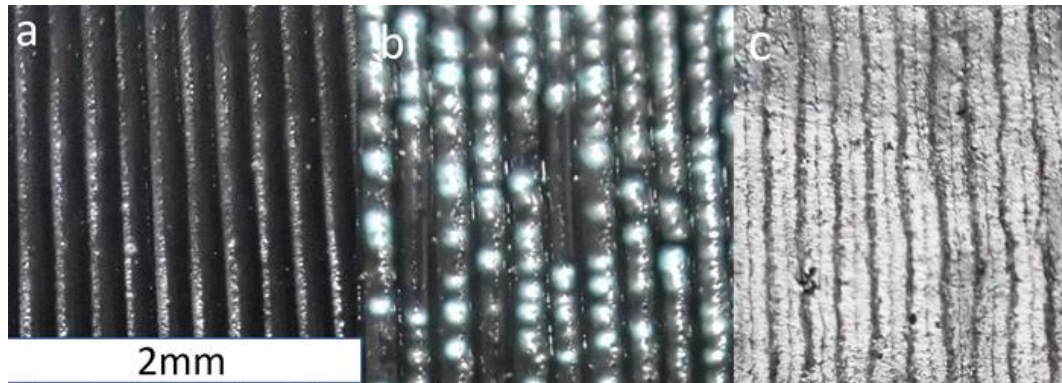


Figure 6.6 Optical image on top, (a) control, (b) 10mm/s 450 mW, (c) 2.5 mm/s 700 mW (same scale bar for all three of them)

The slowest print speed used in this work is 2.5 mm/s, the Ra data of this group is shown in Fig 5 in black square. A clear decrease in Ra is observed starting from 150 mW to 400 mW, then it became steady at around 2  $\mu\text{m}$  with a small fluctuation. The polishing effect was first observed at 200 mW (338 °C from figure 2). The healed surfaces with laser power from 400 mW to 700 mW showed similar surface feature and reflection behavior without variation that can be observed. The optical image of 2.5 mm/s at 700 mW laser

sample is shown in Figure 6 c. Clearly, it can be observed that there is a gap shape region between layers that does not share the same optical behavior. However, physically it is flat as shown in figure 4 d (same sample was used to take optical image). It is assumed that during the surface healing process, the black dye and the PLA polymer behaved differently either in chemical way or physical way, under laser burning and surface reflow.

### 6.3.2 MECHANICAL STRENGTH AND FRACTURE BEHAVIOR

Shown in figure 7 is the tensile strength of laser treated PLA samples and control sample at 5 mm/s. Clearly no major increase or decrease of the tensile strength was observed, except the small drop in tensile strength at 700 mW which is likely to be the result of polymer degradation[52]. Therefore, the effect of laser surface healing process on the mechanical strength is ignorable.

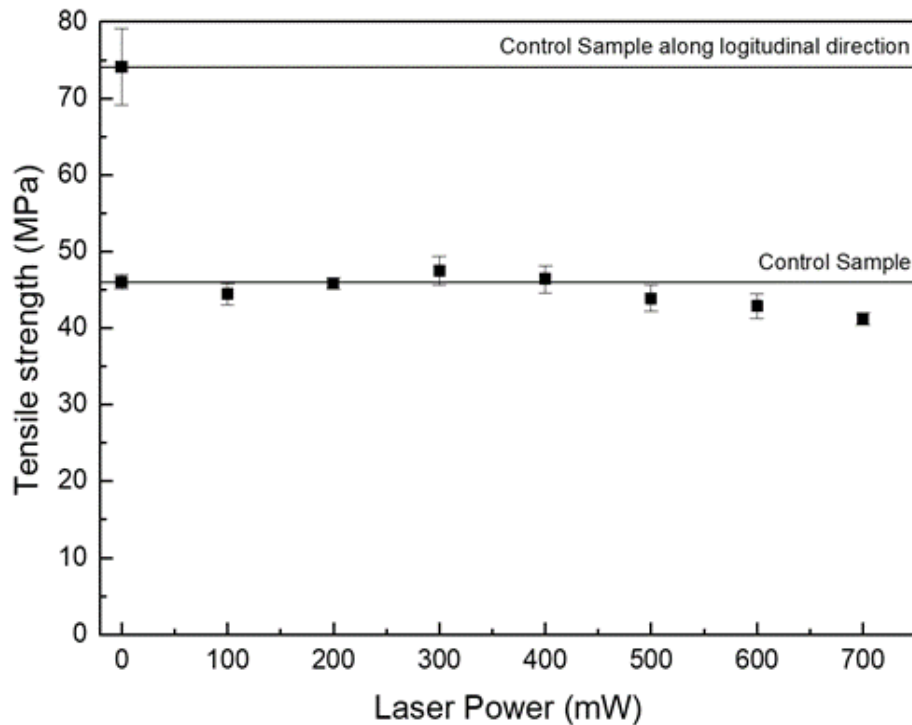


Figure 6.7 Tensile strength of laser treated samples printed at 5mm/s

To further investigate the effect of the laser surface healing process in depth direction (in the direction along laser beam, not along build direction). SEM images were taken on the fracture surface of tensile test samples. Shown in figure a and b are the image for control sample and 700 mW laser sample, respectively. In the control sample, the bottom region, which represents the edge of the deposited track, shows a smooth region without any plastic deformation from fracture. It is the curvature part shown in figure 4 a from the view along build direction. The 700 mW laser sample shows a similar inner fracture feature when compared to the control sample. But a significant different fracture feature was observed at the bottom region (region next to laser healed surface).

The smooth laser healed surface can be partially witnessed at the bottom of figure 8 b. The region next to it shows smoother fracture surface feature compared to the upper region. The upper region, which is similar to one being observed in control sample in figure 8 a, shows numerous plastic deformation but with a small depth. This means a steady bonding has been formed between layers, however the polymer chains near the interface is high stretched and disentangled [41,45,52], the interface is still weak compared to inner layer where the polymer chains are more entangled, therefore polymer chains were pulled out during fracture.

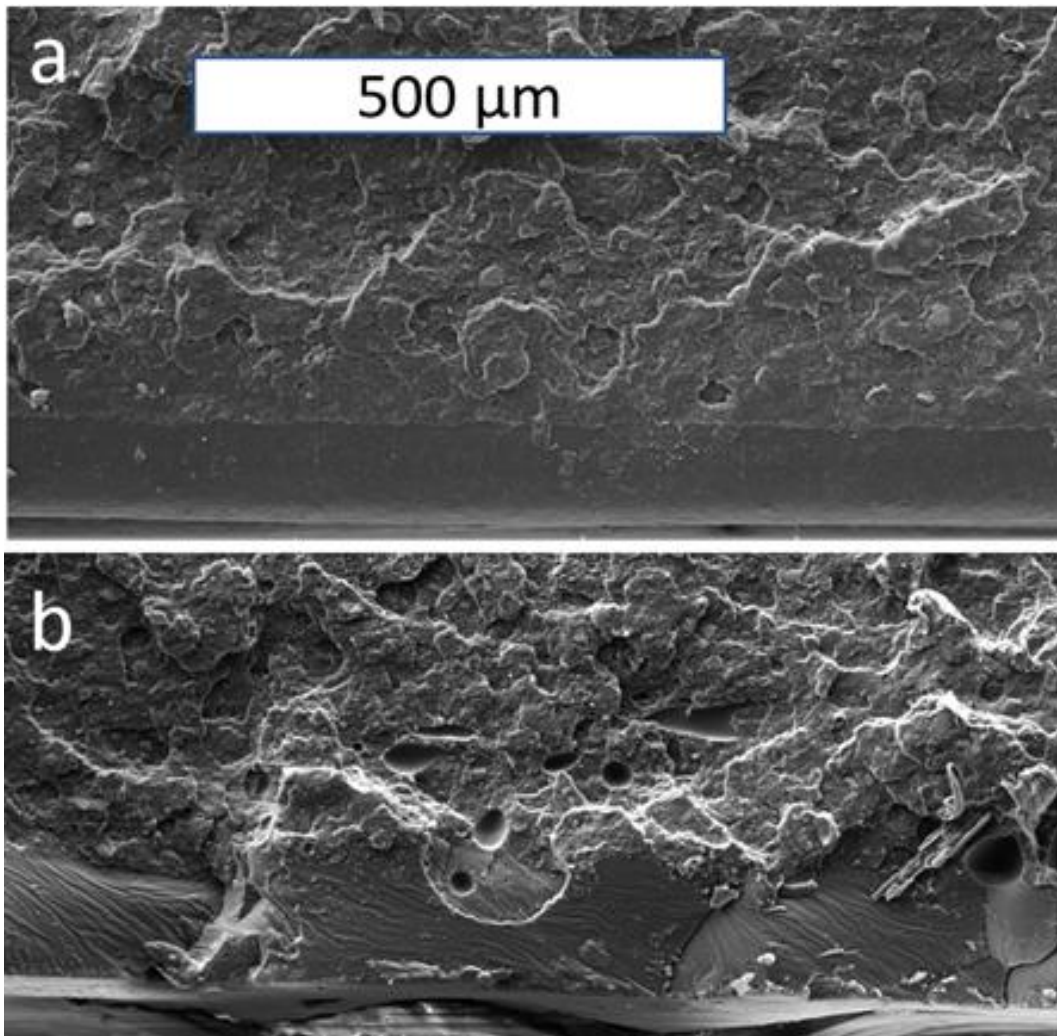


Figure 6. 8 SEM image of fracture surface (a) control sample, (b) Laser sample 5mm/s 700 mW. (Same scale bar is used)

The fracture surface of the region, that were affected by the laser surface healing, however, shows a smoother fracture surface. It indicates that a certain amount of surface reflow was achieved to fulfill the gap between layers, but the time is not sufficient for fully reptation[34] and relaxation[61] to generate a solid and isotropic region. The surface reflow is driven by the surface tension. The depth of the smoother region is comparable with the width of the unbonded region in Fig 8 a. It matches the tensile strength data that this healing process does not have significant effect on mechanical strength.

### 6.3.3 SURFACE HEALING ON CURVED SURFACE

Two customized hose adapters were printed for the performance of the surface healing process on curved surface. Shown in figure 9 is the optical image, with the laser healed adapter on the left and control adapter on the right. This process has performed considerable improvement on surface finish for curved sample.



Figure 6. 9 Optical image of hose adapters printed

### 6.4 CONCLUSIONS

An approach of using laser in-process surface healing to enhance surface finish of fused filament fabricated part was investigated. The effect of laser healing on surface roughness and mechanical strength were observed and discussed. A significant decrease in surface roughness ( $R_a$ ), from 15 micron to 2 micron, was observed. The mechanical strength of

the part was found not to be affected by the surface healing process. This process has shown considerable improvement in surface finish even for curved surface.



## CHAPTER 7

### SUMMARY AND CONCLUSIONS

This dissertation successfully investigates and addresses the mechanical strength issue along all 3 direction and surface roughness issue with FFF built object. The conclusions from this dissertation are summarized below.

- The effect of pre-deposition laser heating process using 10.6  $\mu\text{m}$  laser from 0.33 W to 2 W on the tensile strength and fracture behavior of FFF-printed Ultem 1010 have been investigated. Tensile strength of printed parts in the build direction increased with laser power up to 1.6 W, and reaches 82.8% of that in the print direction (horizontal control sample); equivalent to 178% increase in strength in build direction compared to those in the control samples. This strong inter-layer bonding emerged as a result of increased temperature and time dependent relaxation. It is hypothesized with indirect evidence that the increase in inter-layer strength is due to healing of the interface as a result of higher reptation and entanglement of polymer chains at presence of laser pre-deposition heating. The results markedly highlight the laser pre-deposition heating as a feasible approach to improve the built-part isotropy for the extrusion-based polymer 3D printing processes.
- The effect of laser pre-deposition heating on tensile strength and tensile fracture behavior of FFF-printed PEEK was investigated. Tensile strength of laser pre-heated sample at 2.13 W reaches 80.4 MPa, which is 99.5% of that in in-plane direction,

equivalent to 350.9% increase compared to control sample along build direction. The higher temperature exposure of layer interface and increased time dependent relaxation led to a marked increase in inter-layer bonding strength. Based on indirect evidence, it was speculated that the rising level of inter-layer strength can be attributed to the healing of the interface, which is driven by increased reptation and entanglement of polymer chains under the context of laser pre-deposition heating. Based on these results, laser pre-deposition heating is considered as a viable means of improving the built-part isotropy and their mechanical strength to enhance the extrusion-based polymer 3D printing processes.

- The effect of laser pre-deposition heating process on tensile strength and tensile fracture behavior of FFF-printed PEEK along in-plane direction was presented. Tensile strength of laser pre-deposition heated sample at 1.7 W reached 93.5 MPa, which increased by 11.4% compared to control sample. Laser sample also result in significantly larger elongation before fracture. Besides, necking behavior was observed in laser sample. It is believed that laser enhanced relaxation to happen at intra-layer, therefore increased tensile strength and elongation before fracture. The relaxation appeared to be fully occurred in all laser samples regardless of laser power level. Based on these results, laser pre-deposition heating is considered as a viable means of improving mechanical behavior of parts from extrusion-based 3D printing processes.

- The effect of laser pre-heating on interface healing between adjacent tracks of PLA using fused filament fabrication was investigated. Flexural test was performed on control and laser pre-heating bending samples. The effects of laser pre-heating on flexural behavior and energy microstructure interaction were observed and discussed. An increase of flexural strength between adjacent tracks to up to 106% of that along track direction was found, as well as an increase in displacement before fracture from 50.1% to 68.8%. The effect associated with the use of laser pre-heating are attributed to the thermal-induced increase in polymer reptation and relaxation, therefore resulting in entanglement at the interface between adjacent tracks.
- The effect of laser healing on surface roughness and mechanical strength were observed and discussed. A significant decrease in surface roughness (Ra), from 15 micron to 2 micron, was observed. The mechanical strength of the part was found not to be affected by the surface healing process. This process has shown considerable improvement in surface finish even for curved surface.

## REFERENCES

- [1] B. Brenken, E. Barocio, A. Favaloro, V. Kunc, R.B. Pipes, Fused filament fabrication of fiber-reinforced polymers: A review, *Addit. Manuf.* 21 (2018) 1–16.
- [2] B. Stucker, I. Gibson, D. Rosen, *Additive Manufacturing Technologies*, Springer. (2010).
- [3] L. Li, Q. Sun, C. Bellehumeur, P. Gu, Composite modeling and analysis for fabrication of FDM prototypes with locally controlled properties, *J. Manuf. Process.* 4 (2002) 129–141.
- [4] B. N. Turner, R. Strong, S. A. Gold, A review of melt extrusion additive manufacturing processes: I. Process design and modeling, *Rapid Prototyp. J.* 20 (2014) 192–204.
- [5] N. Hill, M. Haghi, Deposition direction-dependent failure criteria for fused deposition modeling polycarbonate, *Rapid Prototyp. J.* 20 (2014) 221–227.
- [6] D. Drummer, S. Cifuentes-Cuéllar, D. Rietzel, Suitability of PLA/TCP for fused deposition modeling, *Rapid Prototyp. J.* 18 (2012) 500–507.
- [7] C. Ziemian, M. Sharma, S. Ziemian, Anisotropic mechanical properties of ABS parts fabricated by fused deposition modelling, in: *Mech. Eng., InTech*, 2012.
- [8] D. Horvath, R. Noorani, M. Mendelson, Improvement of surface roughness on ABS 400 polymer using design of experiments (DOE), in: *Mater. Sci. Forum*, Trans Tech Publ, 2007: pp. 2389–2392.
- [9] K. Chin Ang, K. Fai Leong, C. Kai Chua, M. Chandrasekaran, Investigation of the mechanical properties and porosity relationships in fused deposition modelling-fabricated porous structures, *Rapid Prototyp. J.* 12 (2006) 100–105.
- [10] T. Nancharaiah, Optimization of process parameters in FDM process using design of experiments, *Int J Emerg Technol.* 2 (2011) 100–102.
- [11] C. Chung Wang, T.-W. Lin, S.-S. Hu, Optimizing the rapid prototyping process by integrating the Taguchi method with the Gray relational analysis, *Rapid Prototyp. J.* 13 (2007) 304–315.
- [12] A.K. Sood, R.K. Ohdar, S.S. Mahapatra, Improving dimensional accuracy of fused deposition modelling processed part using grey Taguchi method, *Mater. Des.* 30 (2009) 4243–4252.

- [13] J.W. Zhang, A.H. Peng, Process-parameter optimization for fused deposition modeling based on Taguchi method, in: *Adv. Mater. Res.*, Trans Tech Publ, 2012: pp. 444–447.
- [14] J. Laeng, Z.A. Khan, S.Y. Khu, Optimizing flexible behaviour of bow prototype using Taguchi approach, *J. Appl. Sci.* 6 (2006) 622–630.
- [15] R.K. Sahu, S.S. Mahapatra, A.K. Sood, A study on dimensional accuracy of fused deposition modeling (FDM) processed parts using fuzzy logic, *J. Manuf. Sci. Prod.* 13 (2013) 183–197.
- [16] A.K. Sood, R.K. Ohdar, S.S. Mahapatra, Parametric appraisal of mechanical property of fused deposition modelling processed parts, *Mater. Des.* 31 (2010) 287–295.
- [17] Y. Zhang, K. Chou, A parametric study of part distortions in fused deposition modelling using three-dimensional finite element analysis, *Proc. Inst. Mech. Eng. Part B J. Eng. Manuf.* 222 (2008) 959–968.
- [18] R. Anitha, S. Arunachalam, P. Radhakrishnan, Critical parameters influencing the quality of prototypes in fused deposition modelling, *J. Mater. Process. Technol.* 118 (2001) 385–388.
- [19] K. Thrimurthulu, P.M. Pandey, N.V. Reddy, Optimum part deposition orientation in fused deposition modeling, *Int. J. Mach. Tools Manuf.* 44 (2004) 585–594.
- [20] B.H. Lee, J. Abdullah, Z.A. Khan, Optimization of rapid prototyping parameters for production of flexible ABS object, *J. Mater. Process. Technol.* 169 (2005) 54–61.
- [21] G.P. Kumar, S.P. Regalla, Optimization of support material and build time in fused deposition modeling (FDM), in: *Appl. Mech. Mater.*, Trans Tech Publ, 2012: pp. 2245–2251.
- [22] F. Rayegani, G.C. Onwubolu, Fused deposition modelling (FDM) process parameter prediction and optimization using group method for data handling (GMDH) and differential evolution (DE), *Int. J. Adv. Manuf. Technol.* 73 (2014) 509–519.
- [23] H.J. O’Connor, D.P. Dowling, Evaluation of the influence of low pressure additive manufacturing processing conditions on printed polymer parts, *Addit. Manuf.* 21 (2018) 404–412.
- [24] F. Lederle, F. Meyer, G.-P. Brunotte, C. Kaldun, E.G. Hübner, Improved mechanical properties of 3D-printed parts by fused deposition modeling processed under the exclusion of oxygen, *Prog. Addit. Manuf.* 1 (2016) 3–7.
- [25] J. Torres, J. Coteló, J. Karl, A.P. Gordon, Mechanical property optimization of FDM PLA in shear with multiple objectives, *Jom.* 67 (2015) 1183–1193.
- [26] S.-H. Ahn, M. Montero, D. Odell, S. Roundy, P.K. Wright, Anisotropic material properties of fused deposition modeling ABS, *Rapid Prototyp. J.* 8 (2002) 248–

257.

- [27] S.H. Masood, K. Mau, W.Q. Song, Tensile properties of processed FDM polycarbonate material, in: *Mater. Sci. Forum*, Trans Tech Publ, 2010: pp. 2556–2559.
- [28] Q. Sun, G.M. Rizvi, C.T. Bellehumeur, P. Gu, Effect of processing conditions on the bonding quality of FDM polymer filaments, *Rapid Prototyp. J.* 14 (2008) 72–80.
- [29] I. Gibson, D.W. Rosen, B. Stucker, Design for additive manufacturing, in: *Addit. Manuf. Technol.*, Springer, 2010: pp. 299–332.
- [30] K. Jud, H.H. Kausch, J.G. Williams, Fracture mechanics studies of crack healing and welding of polymers, *J. Mater. Sci.* 16 (1981) 204–210.
- [31] D.B. Kline, R.P. Wool, Polymer welding relations investigated by a lap shear joint method, *Polym. Eng. Sci.* 28 (1988) 52–57.
- [32] R. Schnell, M. Stamm, C. Creton, Mechanical properties of homopolymer interfaces: Transition from simple pullout to crazing with increasing interfacial width, *Macromolecules.* 32 (1999) 3420–3425.
- [33] P.-G. De Gennes, Introduction to polymer dynamics, CUP Archive, 1990.
- [34] O.A. Ezekoye, C.D. Lowman, M.T. Fahey, A.G. Hulme-Lowe, Polymer weld strength predictions using a thermal and polymer chain diffusion analysis, *Polym. Eng. Sci.* 38 (1998) 976–991.
- [35] R.P. Wool, K.M. O’connor, A theory crack healing in polymers, *J. Appl. Phys.* 52 (1981) 5953–5963.
- [36] T. Ge, F. Pierce, D. Perahia, G.S. Grest, M.O. Robbins, Molecular dynamics simulations of polymer welding: Strength from interfacial entanglements, *Phys. Rev. Lett.* 110 (2013) 98301.
- [37] G. Ćwikła, C. Grabowik, K. Kalinowski, I. Paprocka, P. Ociepka, The influence of printing parameters on selected mechanical properties of FDM/FFF 3D-printed parts, in: *IOP Conf. Ser. Mater. Sci. Eng.*, 2017.
- [38] A. Deshpande, A. Ravi, S. Kusel, R. Churchwell, K. Hsu, Interlayer thermal history modification for interface strength in fused filament fabricated parts, *Prog. Addit. Manuf.* (2018) 1–8.
- [39] A.K. Ravi, A. Deshpande, K.H. Hsu, An in-process laser localized pre-deposition heating approach to inter-layer bond strengthening in extrusion based polymer additive manufacturing, *J. Manuf. Process.* 24 (2016) 179–185.
- [40] H.R. Philipp, D.G. Le Grand, H.S. Cole, Y.S. Liu, The optical properties of a polyetherimide, *Polym. Eng. Sci.* 29 (1989) 1574–1578.
- [41] C. McIlroy, P.D. Olmsted, Deformation of an amorphous polymer during the fused-filament-fabrication method for additive manufacturing, *J. Rheol. (N. Y. N.*

- Y). 61 (2017) 379–397.
- [42] S. Carroccio, C. Puglisi, G. Montaudo, Thermal degradation mechanisms of polyetherimide investigated by direct pyrolysis mass spectrometry, *Macromol. Chem. Phys.* 200 (1999) 2345–2355.
- [43] C. McIlroy, P.D. Olmsted, Disentanglement effects on welding behaviour of polymer melts during the fused-filament-fabrication method for additive manufacturing, *Polymer (Guildf)*. 123 (2017) 376–391.
- [44] A. Tofangchi, P. Han, J. Izquierdo, A. Iyengar, K. Hsu, Effect of Ultrasonic Vibration on Interlayer Adhesion in Fused Filament Fabrication 3D Printed ABS, *Polymers (Basel)*. 11 (2019) 315.
- [45] P. Han, A. Tofangchi, A. Deshpande, S. Zhang, K. Hsu, An approach to improve interface healing in FFF-3D printed Ultem 1010 using laser pre-deposition heating, *Procedia Manuf.* 34 (2019) 672–677.
- [46] H. Zhang, Fire-safe polymers and polymer composites, Office of Aviation Research, Federal Aviation Administration, 2004.
- [47] C.G. Harris, N.J.S. Jursik, W.E. Rochefort, T.W. Walker, Additive Manufacturing with Soft TPU--Adhesion Strength in Multimaterial Flexible Joints, *Front. Mech. Eng.* 5 (2019) 37.
- [48] Y. Wang, J. Shi, Z. Liu, Bending performance enhancement by nanoparticles for FFF 3D printed nylon and nylon/Kevlar composites, *J. Compos. Mater.* (2020) 0021998320963524.
- [49] C. Oztan, S. Ballikaya, U. Ozgun, R. Karkkainen, E. Celik, Additive manufacturing of thermoelectric materials via fused filament fabrication, *Appl. Mater. Today*. 15 (2019) 77–82.
- [50] F. Snijkers, R. Pasquino, P.D. Olmsted, D. Vlassopoulos, Perspectives on the viscoelasticity and flow behavior of entangled linear and branched polymers, *J. Phys. Condens. Matter*. 27 (2015) 473002.
- [51] A.E. Likhtman, T.C.B. McLeish, Quantitative theory for linear dynamics of linear entangled polymers, *Macromolecules*. 35 (2002) 6332–6343.
- [52] P. Han, A. Tofangchi, S. Zhang, A. Deshpande, K. Hsu, Effect of in-process laser interface heating on strength isotropy of extrusion-based additively manufactured PEEK, *Procedia Manuf.* 48 (2020) 737–742.
- [53] S.C. Daminabo, S. Goel, S.A. Grammatikos, H.Y. Nezhad, V.K. Thakur, Fused deposition modeling-based additive manufacturing (3D printing): techniques for polymer material systems, *Mater. Today Chem.* 16 (2020) 100248.
- [54] H. Wu, W.P. Fahy, S. Kim, H. Kim, N. Zhao, L. Pilato, A. Kafi, S. Bateman, J.H. Koo, Recent developments in polymers/polymer nanocomposites for additive manufacturing, *Prog. Mater. Sci.* 111 (2020) 100638.

- [55] C.M. González-Henríquez, M.A. Sarabia-Vallejos, J. Rodríguez-Hernandez, Polymers for additive manufacturing and 4D-printing: Materials, methodologies, and biomedical applications, *Prog. Polym. Sci.* 94 (2019) 57–116.
- [56] M. Spoerk, C. Holzer, J. Gonzalez-Gutierrez, Material extrusion-based additive manufacturing of polypropylene: A review on how to improve dimensional inaccuracy and warpage, *J. Appl. Polym. Sci.* 137 (2020) 48545.
- [57] L.G. Blok, M.L. Longana, H. Yu, B.K.S. Woods, An investigation into 3D printing of fibre reinforced thermoplastic composites, *Addit. Manuf.* 22 (2018) 176–186.
- [58] M. Rafiee, R.D. Farahani, D. Therriault, Multi-material 3D and 4D printing: a survey, *Adv. Sci.* 7 (2020) 1902307.
- [59] G. Verstraete, A. Samaro, W. Grymonpré, V. Vanhoorne, B. Van Snick, M.N. Boone, T. Hellemans, L. Van Hoorebeke, J.P. Remon, C. Vervaet, 3D printing of high drug loaded dosage forms using thermoplastic polyurethanes, *Int. J. Pharm.* 536 (2018) 318–325.
- [60] X. Chen, C. Gao, J. Jiang, Y. Wu, P. Zhu, G. Chen, 3D printed porous PLA/nHA composite scaffolds with enhanced osteogenesis and osteoconductivity in vivo for bone regeneration, *Biomed. Mater.* 14 (2019) 65003.
- [61] P. Han, S. Zhang, A. Tofangchi, K. Hsu, Relaxation of residual stress in fused filament fabrication part with in-process laser heating, *Procedia Manuf.* 53 (2021) 466–471.
- [62] M. Spoerk, F. Arbeiter, H. Cajner, J. Sapkota, C. Holzer, Parametric optimization of intra-and inter-layer strengths in parts produced by extrusion-based additive manufacturing of poly (lactic acid), *J. Appl. Polym. Sci.* 134 (2017) 45401.
- [63] N. Aliheidari, R. Tripuraneni, A. Ameli, S. Nadimpalli, Fracture resistance measurement of fused deposition modeling 3D printed polymers, *Polym. Test.* 60 (2017) 94–101.
- [64] N. Aliheidari, J. Christ, R. Tripuraneni, S. Nadimpalli, A. Ameli, Interlayer adhesion and fracture resistance of polymers printed through melt extrusion additive manufacturing process, *Mater. Des.* 156 (2018) 351–361.
- [65] C.S. Davis, K.E. Hillgartner, S.H. Han, J.E. Seppala, Mechanical strength of welding zones produced by polymer extrusion additive manufacturing, *Addit. Manuf.* 16 (2017) 162–166.
- [66] M. Spoerk, F. Arbeiter, I. Raguž, G. Weingrill, T. Fischinger, G. Traxler, S. Schuschnigg, L. Cardon, C. Holzer, Polypropylene filled with glass spheres in extrusion-based additive manufacturing: effect of filler size and printing chamber temperature, *Macromol. Mater. Eng.* 303 (2018) 1800179.
- [67] J. Yin, C. Lu, J. Fu, Y. Huang, Y. Zheng, Interfacial bonding during multi-material fused deposition modeling (FDM) process due to inter-molecular diffusion, *Mater. Des.* 150 (2018) 104–112.



- [68] V. Srinivas, C.S.J. van Hooy-Corstjens, J.A.W. Harings, Correlating molecular and crystallization dynamics to macroscopic fusion and thermodynamic stability in fused deposition modeling; a model study on polylactides, *Polymer (Guildf)*. 142 (2018) 348–355.
- [69] T.J. Coogan, D.O. Kazmer, Modeling of interlayer contact and contact pressure during fused filament fabrication, *J. Rheol. (N. Y. N. Y)*. 63 (2019) 655–672.
- [70] J.M. Chacón, M.A. Caminero, E. García-Plaza, P.J. Núñez, Additive manufacturing of PLA structures using fused deposition modelling: Effect of process parameters on mechanical properties and their optimal selection, *Mater. Des.* 124 (2017) 143–157.
- [71] A.C. Abbott, G.P. Tandon, R.L. Bradford, H. Koerner, J.W. Baur, Process-structure-property effects on ABS bond strength in fused filament fabrication, *Addit. Manuf.* 19 (2018) 29–38, (n.d.).
- [72] A.P.V. Puerta, S.R. Fernandez-Vidal, M. Batista, F. Girot, Fused deposition modelling interfacial and interlayer bonding in PLA post-processed parts, *Rapid Prototyp. J.* (2019).
- [73] K. Coasey, K.R. Hart, E. Wetzel, D. Edwards, M.E. Mackay, Nonisothermal welding in fused filament fabrication, *Addit. Manuf.* 33 (2020) 101140.
- [74] K.R. Hart, R.M. Dunn, J.M. Sietins, C.M.H. Mock, M.E. Mackay, E.D. Wetzel, Increased fracture toughness of additively manufactured amorphous thermoplastics via thermal annealing, *Polymer (Guildf)*. 144 (2018) 192–204.
- [75] A. Nugroho, R. Ardiansyah, L. Rusita, I.L. Larasati, Effect of layer thickness on flexural properties of PLA (PolyLactid Acid) by 3D printing, in: *J. Phys. Conf. Ser.*, IOP Publishing, 2018: p. 12017.
- [76] X. Gao, S. Qi, X. Kuang, Y. Su, J. Li, D. Wang, Fused filament fabrication of polymer materials: A review of interlayer bond, *Addit. Manuf.* 37 (2021) 101658.
- [77] S.H. Masood, W.Q. Song, Development of new metal/polymer materials for rapid tooling using fused deposition modelling, *Mater. Des.* 25 (2004) 587–594.
- [78] J.F. Christ, N. Aliheidari, A. Ameli, P. Pötschke, 3D printed highly elastic strain sensors of multiwalled carbon nanotube/thermoplastic polyurethane nanocomposites, *Mater. Des.* 131 (2017) 394–401.
- [79] D. Rigotti, A. Dorigato, A. Pegoretti, 3D printable thermoplastic polyurethane blends with thermal energy storage/release capabilities, *Mater. Today Commun.* 15 (2018) 228–235.
- [80] M.D. Nelson, N. Ramkumar, B.K. Gale, Flexible, transparent, sub-100  $\mu\text{m}$  microfluidic channels with fused deposition modeling 3D-printed thermoplastic polyurethane, *J. Micromechanics Microengineering*. 29 (2019) 95010.
- [81] S. Song, A. Wang, Q. Huang, F. Tsung, Shape deviation modeling for fused deposition modeling processes, in: *2014 IEEE Int. Conf. Autom. Sci. Eng.*, IEEE,

2014: pp. 758–763.

- [82] Q. Huang, H. Nouri, K. Xu, Y. Chen, S. Sosina, T. Dasgupta, Predictive modeling of geometric deviations of 3d printed products-a unified modeling approach for cylindrical and polygon shapes, in: 2014 IEEE Int. Conf. Autom. Sci. Eng., IEEE, 2014: pp. 25–30.
- [83] Q. Huang, J. Zhang, A. Sabbaghi, T. Dasgupta, Optimal offline compensation of shape shrinkage for three-dimensional printing processes, *Iie Trans.* 47 (2015) 431–441.
- [84] Y. Jin, Y. He, G. Xue, J. Fu, A parallel-based path generation method for fused deposition modeling, *Int. J. Adv. Manuf. Technol.* 77 (2015) 927–937.
- [85] V. Vijayaraghavan, A. Garg, J.S.L. Lam, B. Panda, S.S. Mahapatra, Process characterisation of 3D-printed FDM components using improved evolutionary computational approach, *Int. J. Adv. Manuf. Technol.* 78 (2015) 781–793.
- [86] Z. Zhu, V. Dhokia, A. Nassehi, S.T. Newman, Investigation of part distortions as a result of hybrid manufacturing, *Robot. Comput. Integr. Manuf.* 37 (2016) 23–32.
- [87] W. Lee, C. Wei, S.-C. Chung, Development of a hybrid rapid prototyping system using low-cost fused deposition modeling and five-axis machining, *J. Mater. Process. Technol.* 214 (2014) 2366–2374.
- [88] P.M. Pandey, N.V. Reddy, S.G. Dhande, Improvement of surface finish by staircase machining in fused deposition modeling, *J. Mater. Process. Technol.* 132 (2003) 323–331.
- [89] D. Ahn, H. Kim, S. Lee, Surface roughness prediction using measured data and interpolation in layered manufacturing, *J. Mater. Process. Technol.* 209 (2009) 664–671.
- [90] D. Ahn, J.-H. Kweon, S. Kwon, J. Song, S. Lee, Representation of surface roughness in fused deposition modeling, *J. Mater. Process. Technol.* 209 (2009) 5593–5600.
- [91] S. Rahmati, E. Vahabli, Evaluation of analytical modeling for improvement of surface roughness of FDM test part using measurement results, *Int. J. Adv. Manuf. Technol.* 79 (2015) 823–829.
- [92] A. Boschetto, L. Bottini, Triangular mesh offset aiming to enhance Fused Deposition Modeling accuracy, *Int. J. Adv. Manuf. Technol.* 80 (2015) 99–111.
- [93] L.M. Galantucci, F. Lavecchia, G. Percoco, Quantitative analysis of a chemical treatment to reduce roughness of parts fabricated using fused deposition modeling, *CIRP Ann.* 59 (2010) 247–250.
- [94] L.M. Galantucci, F. Lavecchia, G. Percoco, Experimental study aiming to enhance the surface finish of fused deposition modeled parts, *CIRP Ann.* 58 (2009) 189–192.

- [95] F. Lavecchia, M.G. Guerra, L.M. Galantucci, Chemical vapor treatment to improve surface finish of 3D printed polylactic acid (PLA) parts realized by fused filament fabrication, *Prog. Addit. Manuf.* (2021) 1–11.
- [96] E. Ukar, A. Lamikiz, L.N.L. de Lacalle, D. Del Pozo, J.L. Arana, Laser polishing of tool steel with CO2 laser and high-power diode laser, *Int. J. Mach. Tools Manuf.* 50 (2010) 115–125.
- [97] A. Gisario, M. Barletta, F. Veniali, Surface reconstruction of porous substrates in sintered bronze by cw-high power diode laser, *Opt. Lasers Eng.* 50 (2012) 1306–1315.
- [98] C.-S. Chang, T.-H. Chen, T.-C. Li, S.-L. Lin, S.-H. Liu, J.-F. Lin, Influence of laser beam fluence on surface quality, microstructure, mechanical properties, and tribological results for laser polishing of SKD61 tool steel, *J. Mater. Process. Technol.* 229 (2016) 22–35.
- [99] S.L. Campanelli, G. Casalino, N. Contuzzi, A.D. Ludovico, Taguchi optimization of the surface finish obtained by laser ablation on selective laser molten steel parts, *Procedia CIRP.* 12 (2013) 462–467.
- [100] M. Taufik, P.K. Jain, Laser assisted finishing process for improved surface finish of fused deposition modelled parts, *J. Manuf. Process.* 30 (2017) 161–177.
- [101] Y. Chai, R.W. Li, D.M. Perriman, S. Chen, Q.-H. Qin, P.N. Smith, Laser polishing of thermoplastics fabricated using fused deposition modelling., *Int. J. Adv. Manuf. Technol.* 96 (2018).
- [102] F. Lambiase, S. Genna, C. Leone, Laser finishing of 3D printed parts produced by material extrusion, *Opt. Lasers Eng.* 124 (2020) 105801.

## CURRICULUM VITAE

NAME: Pu Han

Email: [Pu.Han@louisville.edu](mailto:Pu.Han@louisville.edu)

Cell: 480-295-5734

### EDUCATION

**University of Louisville** 01/2018-12/2021

Major: Mechanical Engineering

Degree: PhD

**Arizona State University** 01/2016-10/2017

Major: Material Science & Engineering Degree

PhD (transferred to UofL)

**Arizona State University** 08/2013-12/2015

Major: Material Science & Engineering

Degree: Master

**Nanchang University** 09/2009-06/2013

Major: Material Physics

Degree: Bachelor

### PUBLICATIONS

Han, Pu, Alireza Tofangchi, Anagh Deshpande, Sihan Zhang, and Keng Hsu. "An approach to improve interface healing in FFF-3D printed Ultem 1010 using laser pre-deposition heating." *Procedia Manufacturing* 34 (2019): 672-677.

Tofangchi, Alireza, Pu Han, Julio Izquierdo, Adithya Iyengar, and Keng Hsu. "Effect of ultrasonic vibration on interlayer adhesion in fused filament fabrication 3D printed ABS." *Polymers* 11, no. 2 (2019): 315.

Han, Pu, Alireza Tofangchi, Sihan Zhang, Anagh Deshpande, and Keng Hsu. "Effect of in-process laser interface heating on strength isotropy of extrusion-based additively manufactured PEEK." *Procedia Manufacturing* 48 (2020): 737-742.

Han, Pu, Sihan Zhang, Alireza Tofangchi, and Keng Hsu. "Relaxation of residual stress in fused filament fabrication part with in-process laser heating." *Procedia Manufacturing* 53 (2021): 466-471.

Han, Pu, Sihan Zhang, Alireza Tofangchi, Julio Jair Izquierdo and Keng Hsu, Development and implementation of in-process, orbiting laser-assisted healing technique on fused filament fabrication (under review)

Han, Pu, Sihan Zhang, Alireza Tofangchi, Julio Jair Izquierdo and Keng Hsu, Interface healing between adjacent tracks in fused filament fabrication using in-process laser heating (under review)

Han, Pu, Sihan Zhang, Alireza Tofangchi, Zhong Yang, Dan Popa, and Keng Hsu., In-process orbiting laser-assisted surface healing in fused filament fabrication (under review)

#### PATENTS

Keng Hsu, Alireza Tofangchi, Pu Han, "Torsional Shear Induced Microstructure & Property Tuning in Extrusion-Based 3D Printed Homogeneous and Composite Materials", US Patent, filed 2019

#### AWARDS

2021 NSF-Sponsored Student Support Awards for NAMRC conference

2019 NSF student travel award for NAMRC conference

2012 1st Class Scholarship by School of Materials Science and Engineering, Nanchang University

2010 2nd Class Scholarship by School of Materials Science and Engineering, Nanchang University